Kinetic fingerprint of antibody therapies
predicts outcomes of Alzheimer clinical trials

Sara Linse[1], Tom Scheidt[2], Katja Bernfur[1], Michele Vendruscolo[2], Christopher M. Dobson[2],

Samuel I. A. Cohen[3], Eimantas Sileikis[1], Martin Lundquist[1], Fang Qian[4], Tiernan O'Malley[4],

Thierry Bussiere[4], Paul H. Weinreb[4], Catherine K. Xu[2], Georg Meisl[2],

Sean Devenish[5], Tuomas P. J. Knowles[2], Oskar Hansson[6]

[1]Biochemistry & Structural Biology, Lund University, Lund, Sweden

[2]Centre for Misfolding Diseases, Department of Chemistry,

University of Cambridge, Cambridge, UK

[3]Wren Therapeutics, Cambridge CB2 8FH, UK

[4]Biogen, Cambridge, Massachusetts 02142, USA

[5]Fluidanalytics, Cambridge, UK

[6]Clinical Memory Research Unit, Department of Clinical Sciences,

Lund University, Lund, Sweden

Address correspondence to Sara Linse: sara.linse@biochemistry.lu.se

or Oskar Hansson: oskar.hansson@med.lu.se

Alzheimer's disease affects nearly 50 million people worldwide with an overall cost of over 1% of the global economy. The amyloid cascade hypothesis, according to which the misfolding and aggregation of the amyloid-β peptide (Aβ) triggers a series of pathological processes that eventually result in massive brain tissue loss (1,2), has driven many therapeutic efforts for the past 20 years. Repeated failures, however, have highlighted the challenges of characterizing the molecular mechanisms of therapeutic candidates targeting Aβ, and connecting them to the outcomes of clinical trials (3-7). Here, we determine the mechanism of action of four clinical stage antibodies (aducanumab, gantenerumab, bapineuzumab and solanezumab). We quantify the dramatic differences that these antibodies have on the aggregation kinetics and on the production of oligomeric aggregates, and link these effects to the affinity and stoichiometry of each antibody for the monomeric

1

and fibrillar forms of Aβ. We show that the binding parameters of each antibody correlate with the corresponding level of amyloid clearance in clinical trials and that the reduction in oligomer flux correlates with the cognitive improvement. We reveal that, uniquely amongst these four antibodies, aducanumab (3) dramatically reduces the flux of oligomeric forms of Aβ. These results demonstrate the power of quantitative molecular analysis in predicting the outcomes of clinical trials.

Amyloid-targeted immunotherapies aim to lower the concentration of Aβ aggregates by promoting their removal through cellular phagocytosis via recruitment of microglia to amyloid plaques, or by directly inhibiting the ongoing aggregation process. Most of these approaches have focused on achieving a global reduction in the concentration of Aβ aggregates or a corresponding delay in the overall Aβ aggregation rate (8). Increasing evidence, however, indicates that different aggregates may have different pathological effects (9,10). In particular, biophysical, cellular and histological data have highlighted the mild toxicity of large fibrillar species, relative to that of oligomeric intermediates of low molecular weight. It is therefore critical to connect the molecular mechanism of potential therapeutics with their effects on the underlying microscopic steps of Aβ aggregation (10,11) since many overall interventions are not likely to affect the levels of the most toxic species generated through this process.

Specifically, studies of the Aβ aggregation mechanism have revealed a multistep process that includes primary nucleation of monomers into aggregates, growth of aggregates by monomer addition and secondary nucleation at fibril surfaces (12). Above a critical but small concentration of fibrils, this latter process becomes the dominant source of new low molecular weight oligomers, which are generated through the nucleation of monomers at the surfaces of existing fibrils (12). Secondary nucleation thereby connects the production of oligomers to the concentrations of both monomers and fibrils. Therefore, there are two fundamental approaches to reduce the flux of oligomeric species: first by directly inhibiting the molecular reaction through which they form, and second by removal of the reactants, including the catalytic fibril surfaces. We present here a strategy based on a quantitative molecular analysis to assess the effects of four clinical stage antibodies, aducanumab, gantenerumab, bapineuzumab and solanezumab in their murine forms

2

[ch]aducanumab, [ch]gantenerumab, 3D6 and m266, respectively, on both of these potential therapeutic modes of action.

First, we assess the potency of the antibodies on the direct inhibition of secondary nucleation using chemical kinetics (10,12,13). The action of an inhibitor is assessed through the global analysis of aggregation reaction time courses (10,11, Fig. S1), which are characterized by a lag-phase, a so-called growth phase and a final plateau. Crucially, all three underlying microscopic processes occur during all three phases, albeit at different rates, as governed by the rate constants and concentrations of reacting species at each point in time (14,15), implying that simple observations of the overall aggregation behavior do not readily allow the changes in molecular mechanisms to be determined. In particular, both elongation and secondary nucleation exhibit their maximum rates during the macroscopic growth phase; the total nucleation rate is highest close to the mid-point ($t_{0.5}$) of the reaction where both fibrils and monomers are present at approximately equal concentrations.

Aggregation of the 42-residue form of Aβ (Aβ$_{42}$) was initiated by a temperature jump from 0 to 37 °C, thus creating supersaturated solutions of Aβ$_{42}$ monomers in the presence or absence of antibodies in pure buffer (Figs. 1 and S2-S5) or in human cerebrospinal fluid (CSF, Fig. S6, 16,17). For each data set, recorded at constant Aβ$_{42}$ concentration and increasing concentrations of each antibody, we performed a fit to the integrated rate law where one of the molecular rate constants k_n, k_2 or k_+ for primary nucleation, secondary nucleation and elongation, respectively, was allowed to vary upon addition of the antibody (16, Fig. 1). Moreover, experiments were conducted in the presence of fixed low (Fig. S7,S8) or high (Fig. 1, first column) concentrations of seeds in the initial reactant solution, thereby bypassing primary or both primary and secondary nucleation to probe specifically the effects on secondary nucleation and/or elongation. All the experiments were run in a blinded manner using the four anti-Aβ antibodies as well as an isotype control antibody.

We found that [ch]aducanumab selectively and dramatically reduces the secondary nucleation rate of Aβ$_{42}$ (Fig. 1A), lowering the effective rate constant for this process by c. 40% even at the lowest concentrations of antibody tested (250 pM, Fig. S4). By contrast, the data show that m266 selectively inhibits primary nucleation (Fig. 1C). For both of these antibodies, no changes are

3

detected to the highly pre-seeded aggregation reaction when high concentrations of antibody are introduced into the reactions, highlighting that the growth of pre-existing aggregates is largely unchanged (Fig. 1). Moreover, the data further indicate that 3D6 and [ch]gantenerumab both act predominantly by reducing the growth of the fibrillar aggregates under both pre-seeded and unseeded reaction conditions (Fig. 1B, 1D). For comparison, the isotype control antibody generates no detectable effect even at high concentration (Fig. S3). In order to extend these findings to physiological conditions, we used CSF in the aggregation assay. In this case, $A\beta_{42}$ displayed an extended lag phase in line with earlier findings (Fig S6, 17,18). However, each antibody was found to predominantly inhibit the same step as in buffer (Fig. 1, S6,S7), with variations in the values of the rate constants related to the complex composition of CSF.

We next verified the reduction in oligomer production from the inhibition of secondary nucleation by direct measurements of the oligomer concentration. To this effect, we quantified the concentration of oligomers present at the half time of the aggregation reaction using MALDI mass spectrometry and size-exclusion chromatography (SEC), after adding a known amount of isotope standard and proteolytic digestion (^{15}N-$A\beta_{42}$) (19, Fig. 2). The results reveal that [ch]aducanumab causes a clear reduction of the free oligomer concentration, in direct agreement with the observed reduction in secondary nucleation, while a smaller reduction is observed with 3D6 and in particular with [ch]gantenerumab, neither of which significantly inhibits secondary nucleation. Interestingly, a fraction of $A\beta_{42}$ elutes together with [ch]aducanumab in the void, most likely representing oligomers bound to [ch]aducanumab (Fig. S9). Direct binding of oligomers can prevent their further conversion to growth-competent fibrils, but can in turn increase their population, although the bound oligomers may be de-toxified by such capture. For m266 we observe a very large amount of $A\beta_{42}$ eluting in early size exclusion chromatography fractions (Fig. S10), consistent with the suggestion that this antibody binds directly to the monomer.

The specific inhibition of secondary nucleation (Fig. 1), and the corresponding reduction in free oligomer concentration (Fig. 2), identified in the presence of [ch]aducanumab implies that this antibody's activity is likely to be driven predominantly by interactions with species unique to secondary nucleation, i.e. the fibril surface, rather than interactions with soluble species which are involved in both primary and secondary nucleation. To verify the molecular species on which this

antibody acts, therefore, we performed experiments in which newly formed Aβ_{42} fibrils, produced in the presence or absence of [ch]aducanumab, were diluted and added to freshly prepared monomer solutions (Fig. S11). We observed that pristine fibrils that had not been exposed to [ch]aducanumab at any stage enhance the process of secondary nucleation and increase the rate of aggregation, whereas pre-formed fibrils that had been generated in the presence of 0.1 molar equivalents of [ch]aducanumab accelerate aggregation to a significantly smaller extent. Kinetic analysis (Fig. S11) reveals a reduction of approximately ca. 33% in the apparent rate constant for secondary nucleation in this latter case, a value that is similar to that identified from the analysis in Fig. 1 (see also Fig. S4), showing that a significant fraction of the inhibitory effect on secondary nucleation originates from interaction of the antibody with fibrillar aggregates.

In order to further investigate the origin of the kinetic inhibition and to assess additional modes of action through reduction in the concentrations of the reactants for secondary nucleation, we probed directly the stoichiometry and affinity of the interactions between each antibody and Aβ_{42} monomers and fibrils. These interactions were investigated through monitoring changes in the molecular diffusion coefficients of the species upon interaction through microfluidic diffusional sizing (20,21). The data reveal that [ch]aducanumab has a low affinity for Aβ_{42} monomers ($K_D = 10\pm7$ μM), but a very high affinity for fibrils ($K_D < 0.9$ nM) with a stoichiometry of one [ch]aducanumab molecule per c.a. 6.2 monomers in the fibril. These findings imply a remarkable specificity ratio of over four orders of magnitude for fibril binding over monomer binding. Interestingly, the width of each antigen-binding region of an IgG is indeed very similar to the summed pitch of 6 planes of a fibril (Fig. S1), and the measured value of the stoichiometry implies that fibrils can become fully coated with [ch]aducanumab along their entire length, which effectively interferes with secondary nucleation at the fibril surface. The remarkable specificity of [ch]aducanumab in suppressing secondary nucleation with no observable effect on elongation (Fig. 1) redirects a significant part of the reactive flux from secondary nucleation to elongation.

The microfluidic diffusional sizing measurements reveal a moderate affinity of [ch]gantenerumab for Aβ_{42} monomers ($K_D = 450$ nM) as well as fibrils ($K_D = 243\pm50$ nM). The stoichiometry of one [ch]gantenerumab per 170 monomers in the fibril (Fig. 2) suggests that [ch]gantenerumab binds to fibrils ends, rationalizing the specific kinetic fingerprint of this antibody in inhibiting fibril growth

5

(Fig. 1). These data are compatible with residues 18-27 forming an essential part of the epitope; several side-chains of this segment are buried in the fibril core and only accessible at the fibril ends (22,23) (Fig. S1). Next, we find relatively a high affinity of 3D6 for $A\beta_{42}$ monomers (K_D = 88±33 nM) as well as fibrils (K_D=5±3 nM) with a stoichiometry of 1 antibody per 32 monomers in the fibril. Finally, for m266 we observe no binding to fibrils but a very high affinity for monomers (K_D = 2±1 nM), which is consistent with its specific suppression of primary nucleation (Fig. 1) and the very large concentration of $A\beta_{42}$ eluting in early fractions as it is likely to be almost exclusively antibody bound (24, Fig. S10).

In addition to direct inhibition of secondary nucleation, a second potential modality of reduction of the oligomer flux is the removal of reactant species required for this process, monomers and fibrils. Monomer removal is likely to be challenging *in vivo* since it would require stoichiometric amounts of antibody to enter the brain, but removal of the catalytic fibril surface is possible at sub-stoichiometric antibody concentrations. This latter process requires a significant fibril-bound antibody population; the binding analysis reveals that [ch]aducanumab has a dissociation constant for fibril interactions below 1 nM, and is significantly more specific to aggregated species than the other clinical antibodies (Fig. 3C).

Finally, we investigate the connection between the quantitative molecular analysis and the outcomes for the clinical trials for the four antibodies. Our results demonstrate that detailed kinetic analyses carried out *in vitro* in the early stages of preclinical development establish the mechanism of action of the antibodies and enable accurate predictions of the outcomes of clinical trials (Fig. 4). Specifically, we found that a measure of the fraction of antibodies bound to amyloid fibrils correlates with the level of clearance of amyloid plaques in treated patients (Fig. 4A). This effect arises from the microglia-directing activity associated with the effector function of the antibodies bound to the fibrils. Furthermore, the reduction of the oligomer production rate correlates with the second key readout from clinical trials, the level of cognitive improvement in treated patients (Fig. 4B). We thus propose that a quantitative molecular analysis considering the fraction of antibody bound and the oligomer flux (Fig. 4C, squares) can predict plaque clearance and cognitive improvement (Fig. 4C, shaded ellipses).

Supplementary Information is available for this paper.

DISCLOSURES

SL acquired research support (for the institution) from Biogen to cover the costs for the kinetic experiments and analyses as well as the oligomer generation experiments and analyses. OH has acquired research support (for the institution) from Roche, GE Healthcare, Biogen, AVID Radiopharmaceuticals and Euroimmun. In the past 2 years, he has received consultancy/speaker fees from Biogen and Roche. SL, SC, MV, CMD, TPJK are founders of Wren Therapeutics Ltd.

NOTE ADDED WITH SUBMISSION

On 22 October 2019, Biogen announced their intention to file for regulatory approval of aducanumab in Alzheimer's disease.

AUTHOR CONTRIBUTIONS

SL, OH designed the study. SL expressed and purified recombinant Aβ1-42 and Aβ(MC1-42) peptides. SL, ML and ES developed and optimized the protocol for recombinant Aβ1-42 production and purification. FQ, TO'M, TB and PHW generated and purified the antibodies. OH provided the pooled CSF samples. SL isolated $A\beta_{42}$ monomers and antibodies by SEC and performed the aggregation kinetics experiments before unblinding. SL performed kinetic analysis of the data before unblinding. GM performed additional kinetic analysis of the data after unblinding. SL produced and purified the Alexa647-labelled forms of Aβ42 and all antibodies. SL performed the oligomer quantification experiments, and KB performed all mass spectrometry analyses before unblinding. TS performed the diffusion measurements of K_D and stoichiometry before unblinding. SL, TS, SD, CKX and GM analysed the diffusion data. MV, SC, TPJK correlated the kinetics results with clinical data. SL, MV, SC, TPJK, OH wrote the paper with input from all co-authors.

REFERENCES

1. Hardy, J. & Higgins, G. Alzheimer's disease: the amyloid cascade hypothesis. *Science* **256**, 184–185 (1992).

2. Selkoe, D.J. & Hardy, J. The amyloid hypothesis of Alzheimer's disease at 25 years. *EMBO Mol Med.* **8**, 595-608 (2016).

3. Sevigny J. *et al.* The antibody aducanumab reduces Aβ plaques in Alzheimer's disease. *Nature* **537**, 50–56 (2016).

4. Bohrmann B., *et al.*, Gantenerumab: a novel human anti-Aβ antibody demonstrates sustained cerebral amyloid-β binding and elicits cell-mediated removal of human amyloid-β. *J. Alzheimer's Dis.* **28**, 49 (2012).

5. Ostrowitzki, S. *et al.* SCarlet RoAD Investigators, A phase III randomized trial of gantenerumab in prodromal Alzheimer#s disease. *Alzheimers Res. Ther.* 9, 95 (2017).

6. L.S. Honig, L.S. *et al.* Trial of solanezumab for mild dementia due to Alzheimer's disease. New. Eng. Medicine **378**, 321-330 (2018).

7. Salloway, S. *et al.* Two phase 3 trials of bapineuzumab in mild-to-moderate Alzheimer's disease. N Engl J Med. 370(4):322-33 (2014).

8. Härd, T. & Lendel, C. Inhibition of amyloid formation. *J. Mol. Biol.* 421, 441-465 (2012).

9. Walsh, D.M. *et al.* Naturally secreted oligomers of amyloid beta protein potently inhibit hippocampal long-term potentiation in vivo. *Nature* **416**, 535-539 (2002).

10. Cohen, S.I.A. *et al.* A molecular chaperone breaks the catalytic cycle that generates toxic Aβ oligomers. *Nat. Struct. Mol. Biol.* **22**, 207-213 (2015).

11. Arosio, P. *et al.* Kinetic analysis reveals the diversity of microscopic mechanisms through which molecular chaperones suppress amyloid formation. *Nat. Commun.* **7**, 10948 (2016).

13. Knowles, T.P. *et al.*. An analytical solution to the kinetics of breakable filament assembly. *Science* **326**, 1533-1537 (2009).

12. Cohen, S.I. *et al.* Proliferation of amyloid-β42 aggregates occurs through a secondary nucleation mechanism. *Proc. Natl. Acad. Sci. U. S. A.* **110**, 9758-9763 (2013).

14. Cohen, S.I., Vendruscolo, M., Dobson, C.M. & Knowles, T.P. From macroscopic measurements to microscopic mechanisms of protein aggregation. *J. Mol. Biol.* **421**, 160-171 (2012).

8

15. Arosio, P., Knowles, T.P. & Linse, S. On the lag phase in amyloid fibril formation. *Phys. Chem. Chem. Phys*. **17**, 7606-18 (2015).

16. Meisl, G. *et al*. Molecular mechanisms of protein aggregation from global fitting of kinetic models. *Nat. Protoc*. **11**, 252-272 (2016).

17. Padayachee, E.R. *et al*. Cerebrospinal fluid-induced retardation of amyloid β aggregation correlates with Alzheimer's disease and the APOE ε4 allele. *Brain Res.* **1651**, 11-16 (2016).

18. Frankel, R. *et al*. Autocatalytic amplification of Alzheimer-associated Aβ42 peptide aggregation in human cerebrospinal fluid. *Nature Commun. Biol.* **2**, 365 (2019).

19. Michaels, T.C.T. *et al*. Dynamics of oligomer populations formed during the aggregation of Alzheimer's Aβ42 peptide. *Nat. Chem.* resubmitted and in re-review.

20. Arosio, P. *et al*. Microfluidic Diffusion Analysis of the Sizes and Interactions of Proteins under Native Solution Conditions. *ACS Nano* 10, 333-41 (2016).

21. Yates, E.V. *et al*. Latent analysis of unmodified biomolecules and their complexes in solution with attomole detection sensitivity. *Nat. Chem.* **7**, 802-809 (2015).

22. Colvin, M.T. *et al*. Atomic Resolution Structure of Monomorphic Aβ42 Amyloid Fibrils. *J Am Chem Soc* **138**, 9663-9674 (2016).

23. Wälti, M.A. *et al*. Atomic-resolution structure of a disease-relevant Aβ(1-42) amyloid fibril. *Proc. Natl. Acad. Sci. U.S.A.* **113**, E4976-4984 (2016).

24. Arndt J.W. *et al*. Structural and kinetic basis for the selectivity of aducanumab for aggregated forms of amyloid-β. *Sci. Rep.* **8**, 6412 (2018).
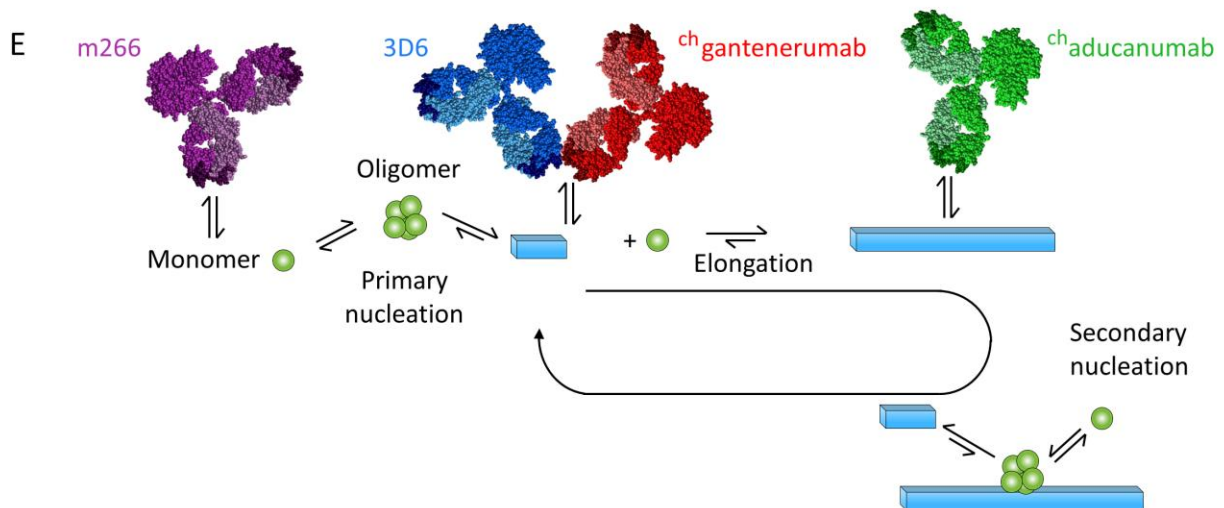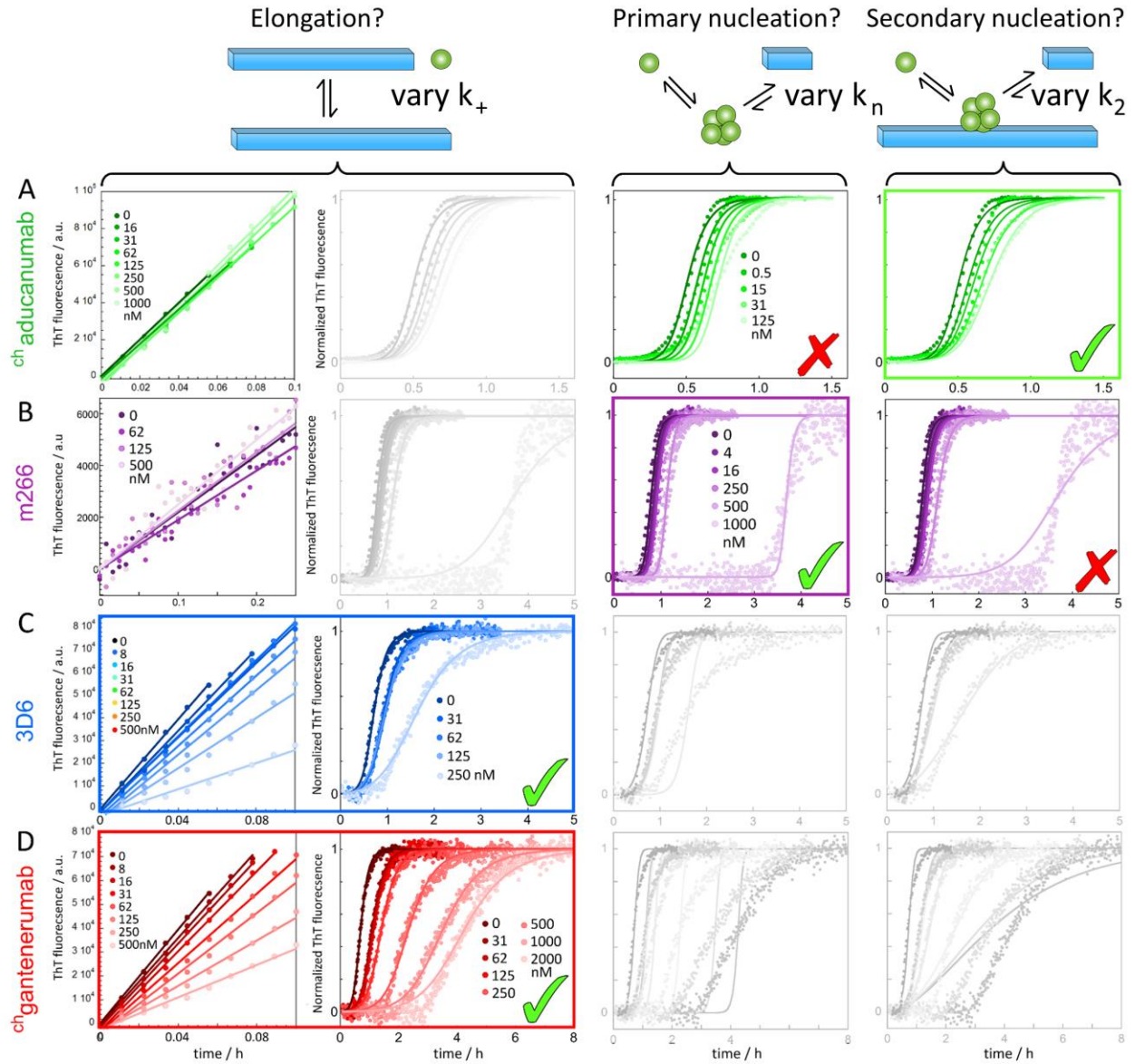
Figure 1. Effects of the antibodies on the kinetics of aggregation of Aβ42. (A-D) Thioflavin T (ThT) fluorescence as a function of time for reactions starting from 3-4 μM recombinant Aβ1-42 in 20 mM HEPES/NaOH, 140 mM NaCl, 1 mM CaCl$_2$, pH 8.0 in the absence and presence of ^{ch}aducanumab (**A**) m266 (**B**), 3D6 (**C**) or ^{ch}gantenerumab (**D**). The colour codes for the antibody concentrations in nM are given on each row. The data are shown in normalized form, with the non-normalized data in Fig. S3. Data in the presence of isotype control are shown in Fig. S3. The solid lines are fits to the data and assume in the left column global values for k$_2$ and k$_n$ and curve-specific values for k$_+$, in the middle column global values for k$_+$ and k$_n$ and curve-specific values for k$_{2,}$ and in the right column global values for k$_2$ and k$_+$ and curve-specific values for k$_2$. The best fit in each case is indicated by a green tick. Note that the x-axis covers 2, 5 or 8 h depending on the magnitude of the effect of each antibody. Data and analysis for additional concentrations of each antibody are shown in Fig. S3 and S4. (**E**) Schematic illustration of the different microscopic steps in the aggregation that are primarily affected by the four antibodies.
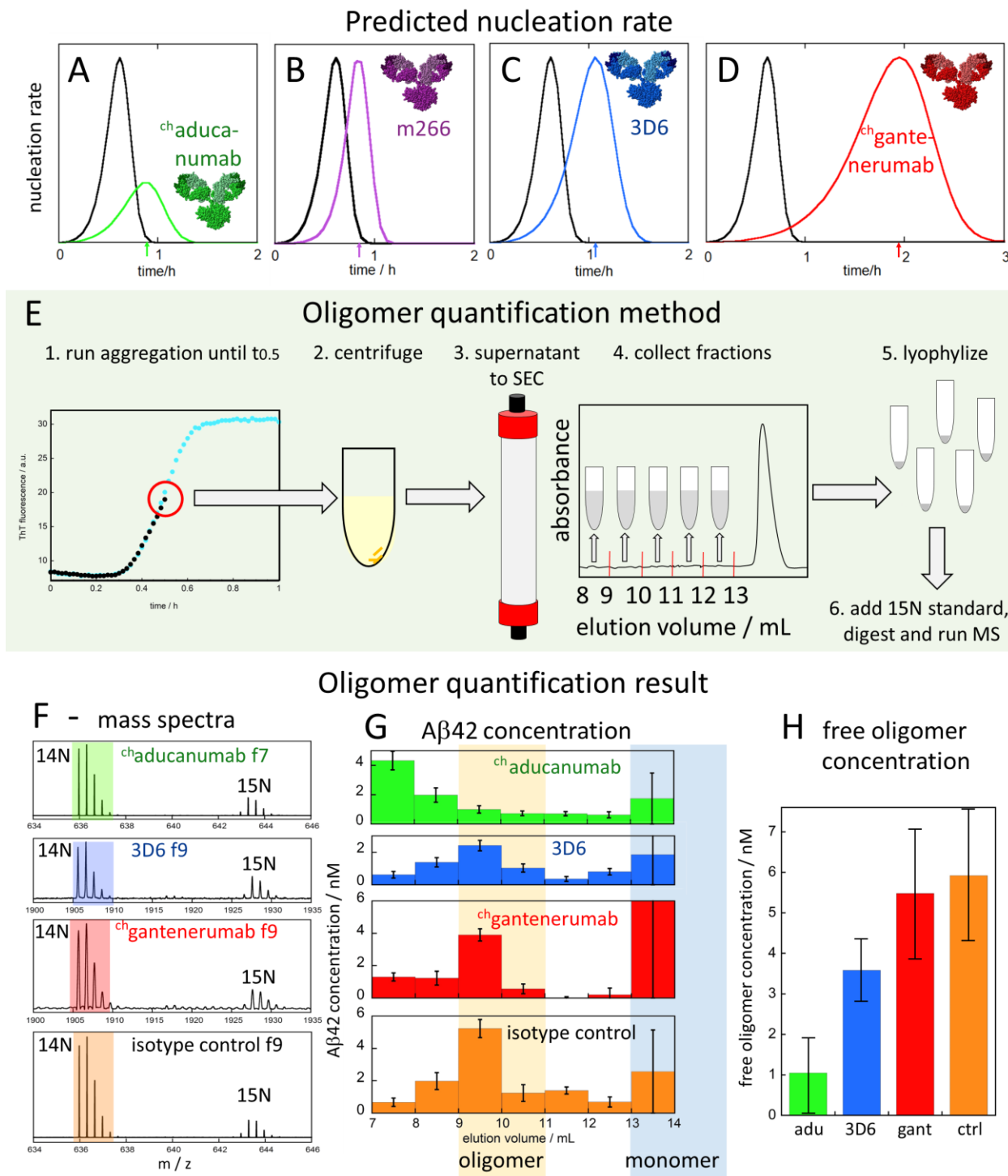
11

Figure 2. Effects of the antibodies on the production of Aβ42 oligomers. (**A-D**) Predicted effects of the four antibodies on the Aβ1-42 nucleation rate based on fitted rate constants. The arrows on the time axis point to t_{half} of the macroscopic aggregation curve. (**E**) Outline of the oligomer

quantification experiment. Samples were collected at t_{half}, the point in time where the ThT fluorescence was half-way in between the baseline and plateau values for each respective reaction. The samples were centrifuged, the supernatant separated by SEC and 1 mL fractions collected from the void to the start of the monomer peak, lyophilized, supplemented with 1 nM ^{15}N-Aβ(M1-42) as an isotope standard, digested and analysed by mass spectrometry. (**F**) Examples of data showing the DSGYEVHHQKLVFFAE peptide pair where the ^{14}N peptide has a monoisotopic mass of 1905.91 Da and the ^{15}N peptide a mass of 1927.91 Da. These two peptides are chemically equivalent and can be used for quantification. Example data for one fraction (f) from reactions in the presence of isotope control (f9), ^{ch}aducanumab (f7), ^{ch}gantenerumab (f9), and 3D6 (f9). (**G**) Observed size distribution of oligomers from one experiment. (**H**) Free oligomer concentration eluting from samples collected at $t_{1/2}$ in the presence of each antibody. The data shown are averages of fraction 9+10 from two repeats and the error bars include the values in both repeats plus estimated maximum fraction collection errors. The data for m266 are not included in the graph since in this case a very large amount of Aβ1-42 elutes together with the antibody in the column void (Fig. S10).
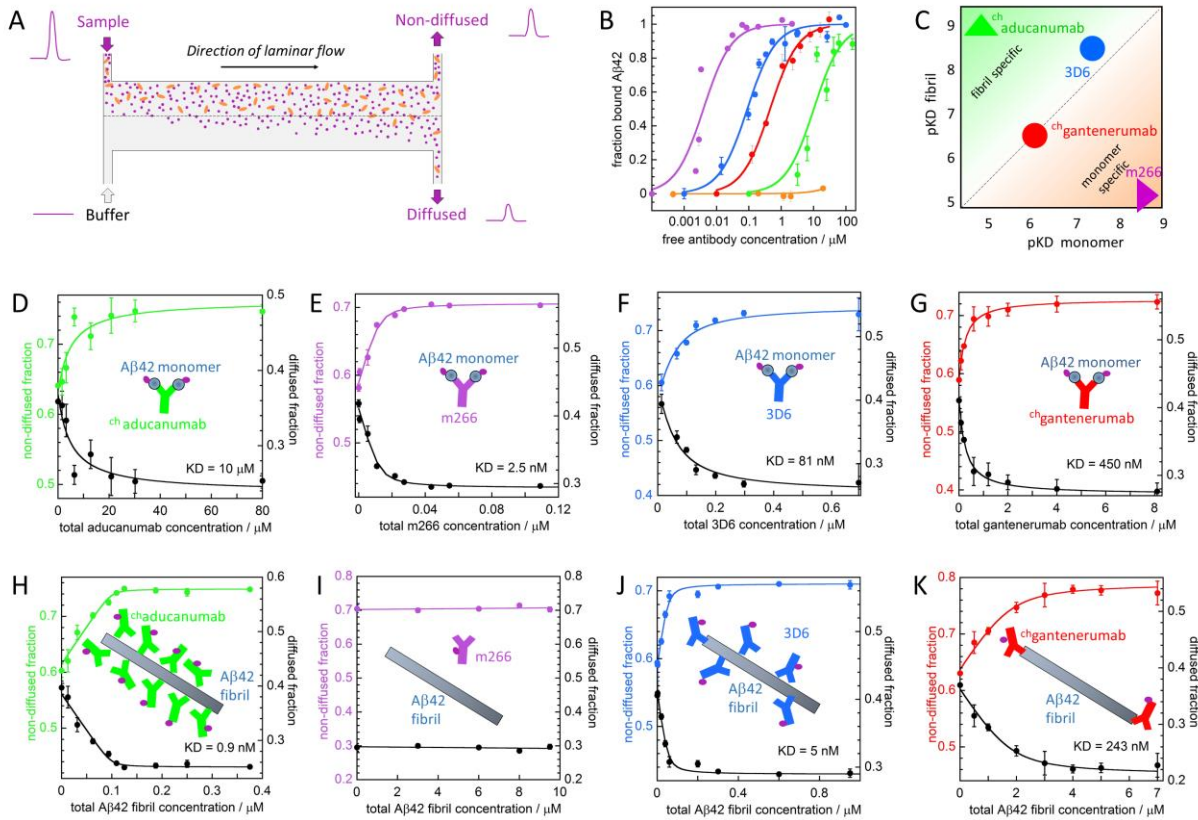
Figure 3. Binding affinity of the antibodies to Aβ42 monomers and fibrils. (**A**) Principle of diffusion-based sizing of Alexa467-labelled species (purple) in the presence of an interaction partner (orange). The dashed line indicates the middle of the channel. (**B**) Monomer saturation versus antibody concentration, calculated from the fits in panels D-G. (**C**) Summary of the obtained affinities of each antibody for monomers and fibrils, expressed as $pKD = -log_{10}(K_D)$. (**D-G**) Diffusion of Alexa467-Aβ(MC1-42) monomers in the absence and presence of increasing concentrations of each antibody. (**H-K**) Diffusion of Alexa467-antibodies in the absence and presence of increasing concentrations of unlabeled Aβ1-42 fibrils. Data for ^{ch}aducanumab are in **D,H**; m266 **E,I**; 3D6 **F,J**; ^{ch}gantenerumab **G,K**. Data for isotype control are in Fig. S12. All data were analysed by fitting directly to the observed distribution of fluorescent species at the end of the microfluidic channel. The data in panels D-G were fitted assuming a fixed stoichiometry of 2 monomer binding sites per antibody, and with three adjustable parameters: K_D and the fractions of each state (free and bound) in the respective channel. The data in panels H-K were fitted with four adjustable parameters: stoichiometry, K_D and the fraction of each state (free and bound) in the

14

respective channel. Note that the measured fraction in the diffused channel is equal to one minus the fraction in the non-diffused channel.
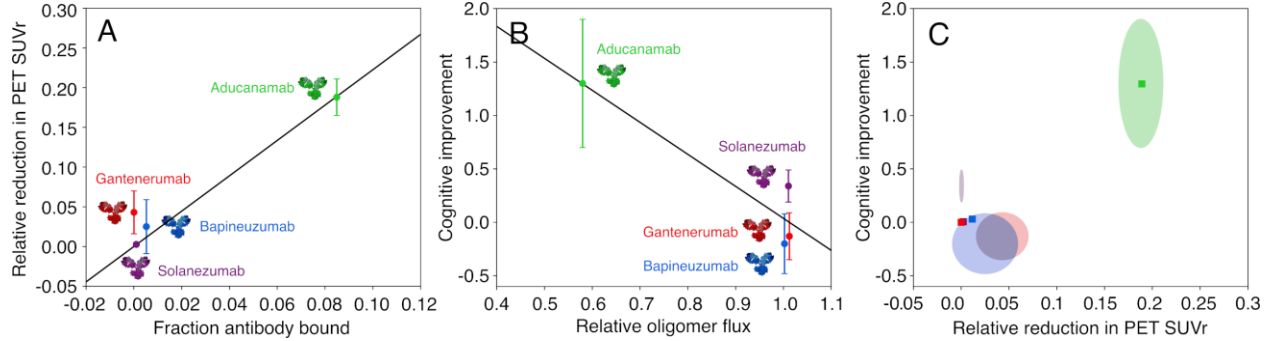
Figure 4. From the mechanism of action to the outcome of the clinical trials. (A) The fraction of antibodies bound to amyloid fibrils correlates with the level of clearance of amyloid plaques in patients treated in clinical trials. **(B)** The reduction of the oligomer production rate (oligomer flux) correlates with the level of cognitive improvement in treated patients. Note that since the aggregation process involves Aβ simultaneously acting as reactant, product, intermediate and catalyst, antibodies may reduce the levels of Aβ oligomers even without binding them directly. **(C)** Taken together, the fraction of antibody bound and the oligomer flux can predict plaque clearance and cognitive improvement. The points show the predictions for aducanumab (green), solanezumab (purple), bapineuzumab (blue) and gantenerumab (red) based on the straight line fits in panels A and B, and the shaded ellipses show the clinical data (with their standard errors) as displayed in panels A and B.
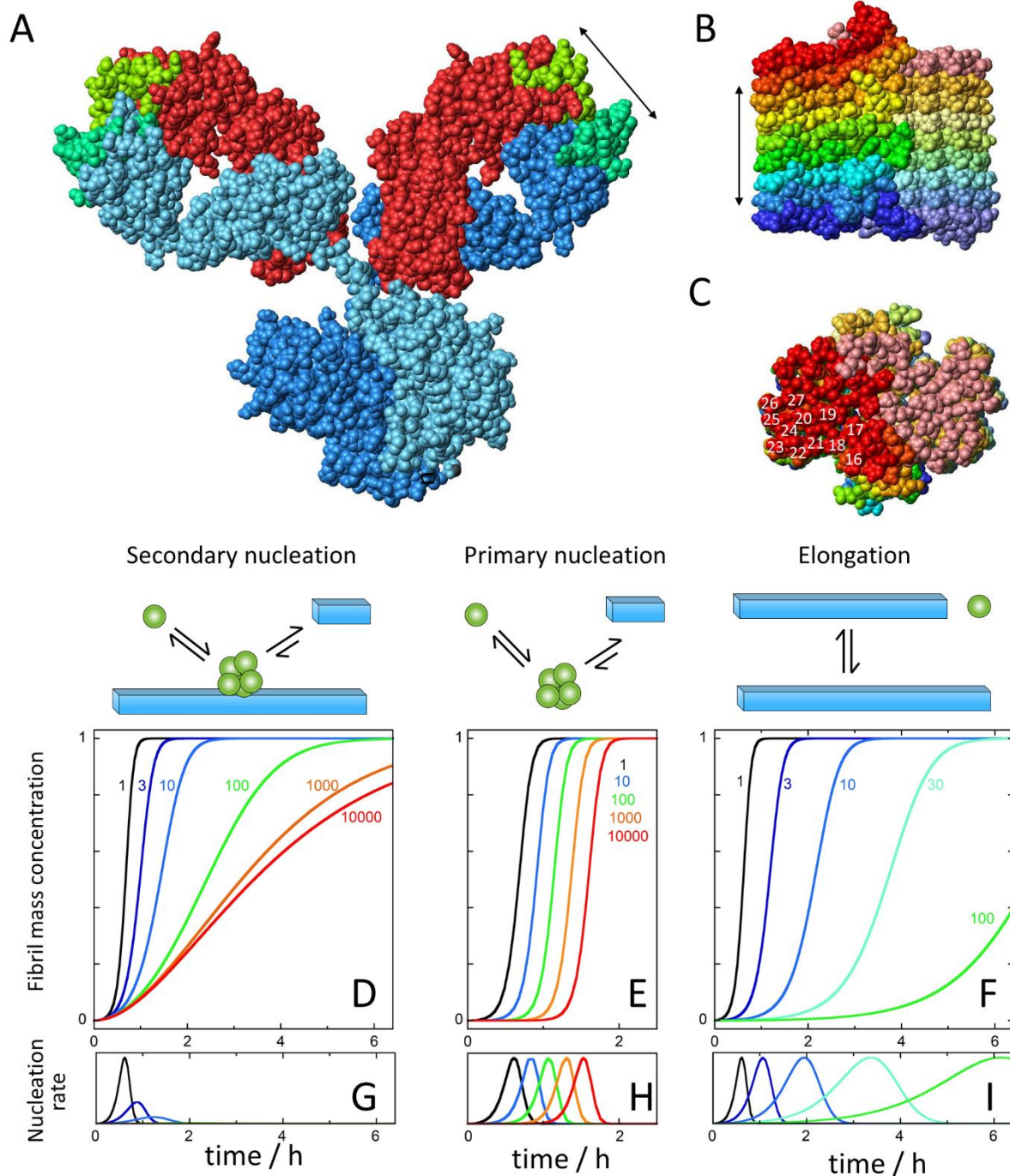
Figure S1. Comparison of the sizes of a full-length IgG and Aβ₄₂ fibrils, and theoretical aggregation curves and nucleation rates. Structure of a full-length IgG (1igy.pdb, **A**) with the heavy chains in blue, light chains in red and variable loops in green. (**B**,**C**) Structure of a short section. 9 planes, of an Aβ₄₂ fibril (5kk3.pdb (22), drawn in the same scale as IgG. In panel **B**, the fibril is viewed from the side; each plane contains two monomers in darker and paler colour. In panel **C** the fibril is viewed from the top with the location of residue 16-27 side-chains indicated in one of the monomers. The models in panel B and C are related by a 90° rotation and residues

17

11-42 are shown. The rest of the N-terminus is less ordered and not included in the ssNMR structure, but would extend at the top and bottom in panel **C**, and towards and away from the viewer in panel **B**. The double-headed arrow in panels **A** and **B** corresponds to 2.7 nm. (**D-F**) Predicted changes to the macroscopic aggregation curve if the rate constant for one specific microscopic step is selectively reduced by a factor of 3 (marine blue), 10 (blue), 30 (cyan), 100 (green), 1000 (orange) or 10000 (red). The reference curve is calculated for 3 µM Aβ42 in 20 mM Hepes,140 mM NaCl, 1 mM CaCl$_2$ pH 8.0 (18) with $k_nk_+ = 2.5 \cdot 10^{-3}$ M^{-2}s^{-2}, $k_2k_+ = 2.1 \cdot 10^{13}$ M^{-3}s^{-2}, $\sqrt{K_M} = 0.25$ µM; $n_c = 1$, $n_2 = 2$. (**D-F**) Selective inhibition of: secondary nucleation (**D**), primary nucleation (**E**), and elongation (**F**). The total nucleation rate underlying each trace in panel **D**, **E** and **F** is shown in panel **G**, **H**, and **I**, respectively. Note that since the macroscopic curves are sensitive to the rate constant products (k_nk_+ and k_2k_+, 10) precicely the same effect as displayed in panel F can in principle arise if both k_n and k_2 are reduced in parallel by the same factor.
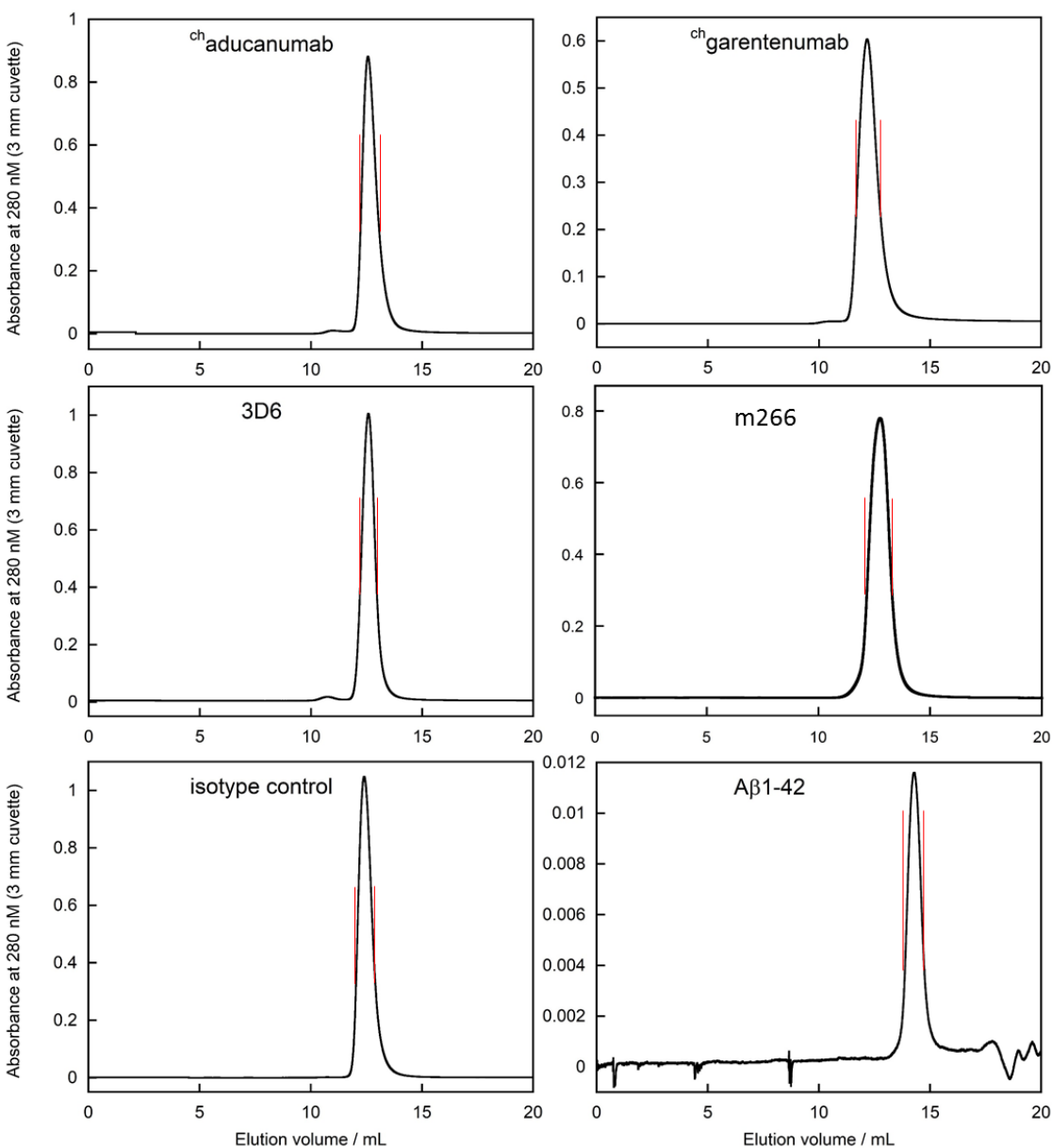
Figure S2. Isolation of monomeric Aβ42 and antibodies by size exclusion chromatography. Isolation of the antibodies on a 1 x 30 cm Superdex 200 column (GE healthcare) in 20 mM HEPES/NaOH, 150 mM NaCl, 1 mM CaCl2, pH 8.0 just prior to the kinetics experiment (first five panels). Isolation of recombinant Aβ1-42 on a 1 x 30 cm Superdex 75 column (GE healthcare) in 20 mM HEPES/NaOH, 1 mM CaCl2, pH 8.0 just prior to the kinetics experiment (last panel). 140 mM NaCl was added from a 4.2 M NaCl stock after size exclusion to limit losses on the column. In each case, the fraction between the vertical red lines was collected.
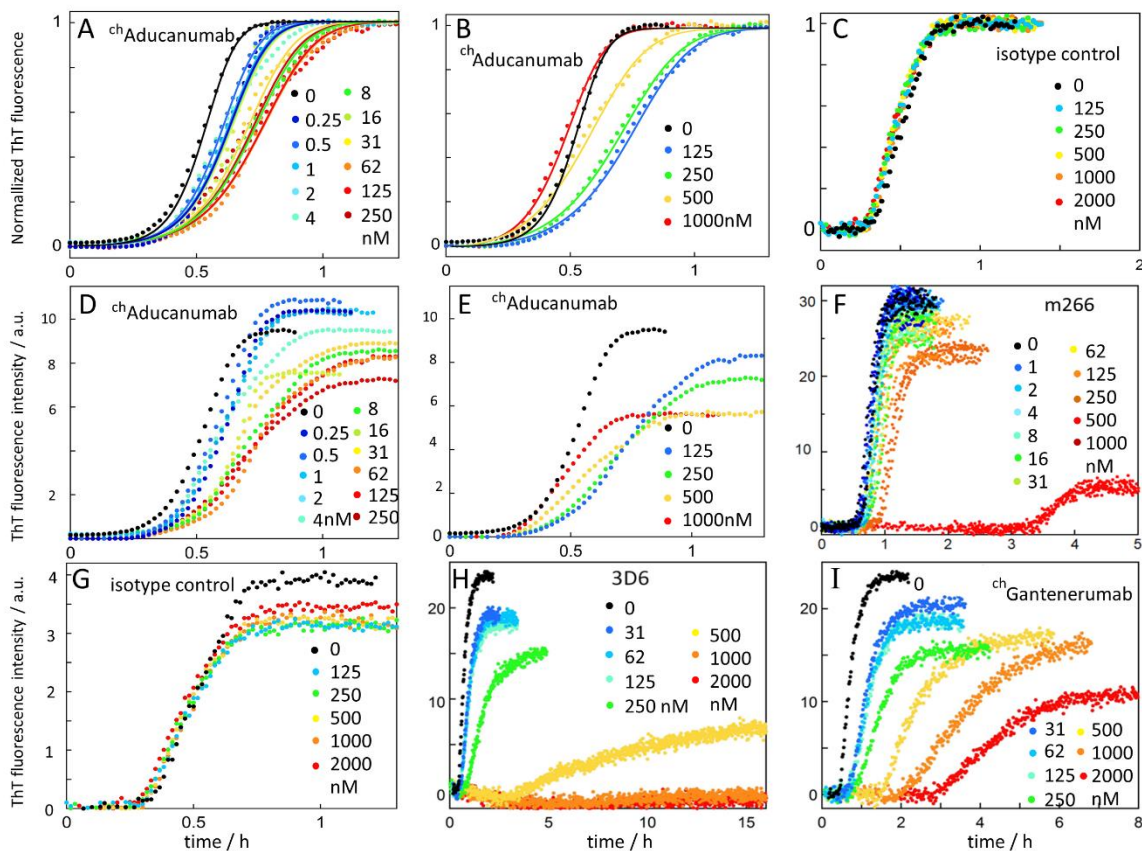
19

Figure S3. Aggregation kinetics data of Aβ1-42 in the absence and presence of antibodies. All panels show data acquired using recombinant Aβ1-42 at 37 °C under quiescent conditions in 20 mM Hepes/NaOH, 140 mM NaCl, 1 mM $CaCl_2$, pH 8.0 in PEGylated plates. (**A-C**) Normalized data with ^chaducanumab (**A,B**) and isotype control (**C**). The same data are shown in non-normalized form in panels (**D,E**) and (**G**), respectively. Panels (**F, H**, **I**) show the same data as shown in Fig. 1, and in addition panel **H** includes data at 500-2000 nM 3D6. The fitted lines in panel A are with reduced values of k_2. The fits in panel B, to normalized data in the absence and presence 250 -1000 nM ^chaducanumab, allow for a decrease in k_2 and an increase in k_n.

We note that at very high concentrations (>500 nM), which are unlikely to be realized *in vivo*, ^chaducanumab accelerates the bulk Aβ42 aggregation process by increasing the primary nucleation rate. Indeed, the data at 250-1000 nM aducanumab are best fitted assuming that the effect on k_2 is combined with an increase in k_n (Fig. S4) Interestingly, at high concentrations of each antibody, the ThT intensity is significantly reduced, which for m266 and 3D6, is found to be related to a significant concentration of Aβ1-42 remaining in solution (Fig. S5), implying the possibility of monomer binding which we assess directly in solution (Fig. 3).
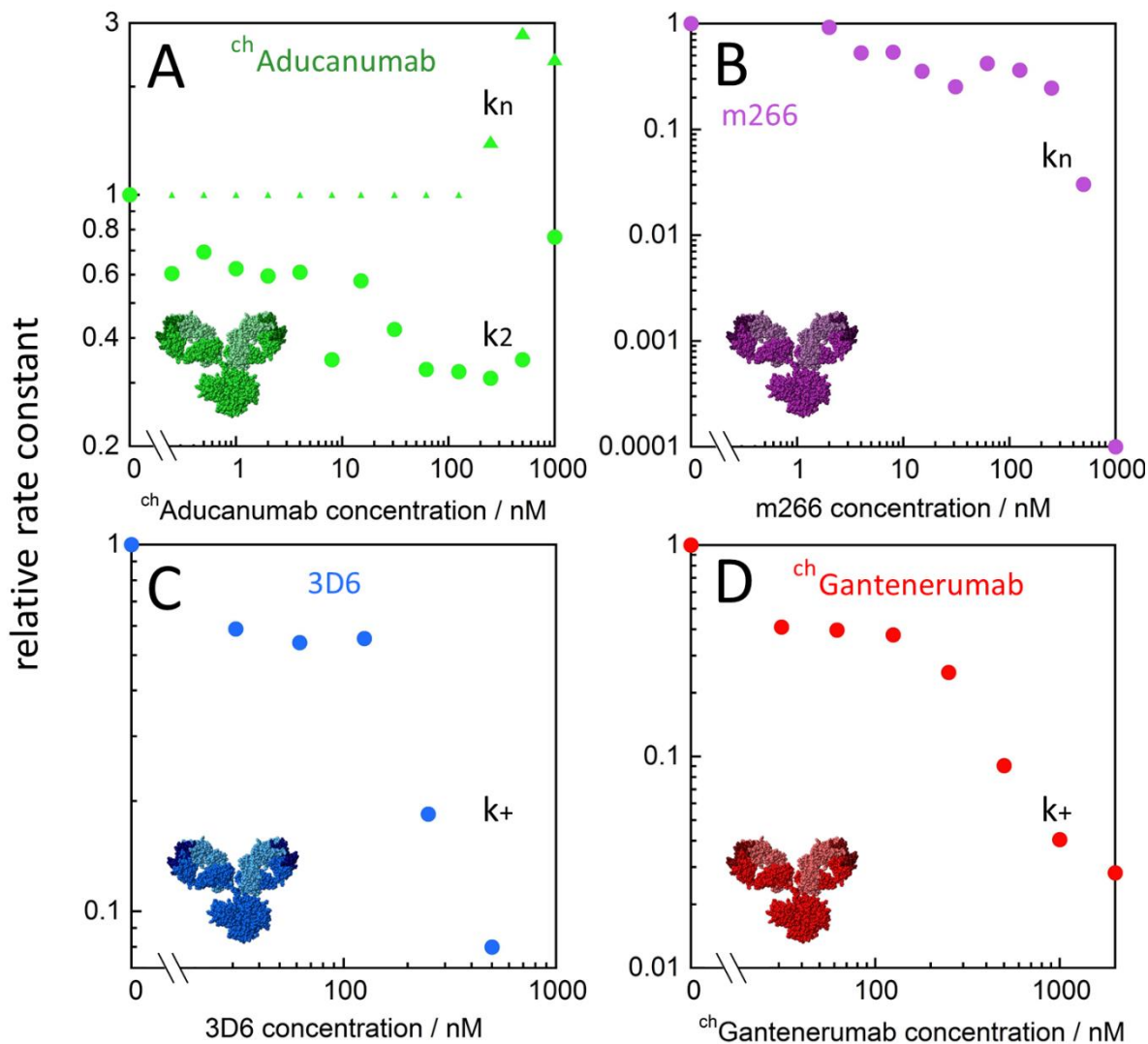
20

Figure S4. Effects of the antibodies on the rate constants. The rate constant values relative to Aβ42 alone are shown as a function of the antibody concentration for the case that produced the best fit to the data for each antibody (see Fig. 1). For ^{ch}aducanumab (**A**) we thus show the effect on the rate constant for secondary nucleation, k_2, up to 125 nM antibody, and thereafter the effects in k_n and k_2. For m266 (**B**) we show the effect on the rate constant for primary nucleation, k_n. For 3D6 (**C**) and ^{ch}gantenerumab (**D**) we show the effect on the elongation rate constant, k_+.
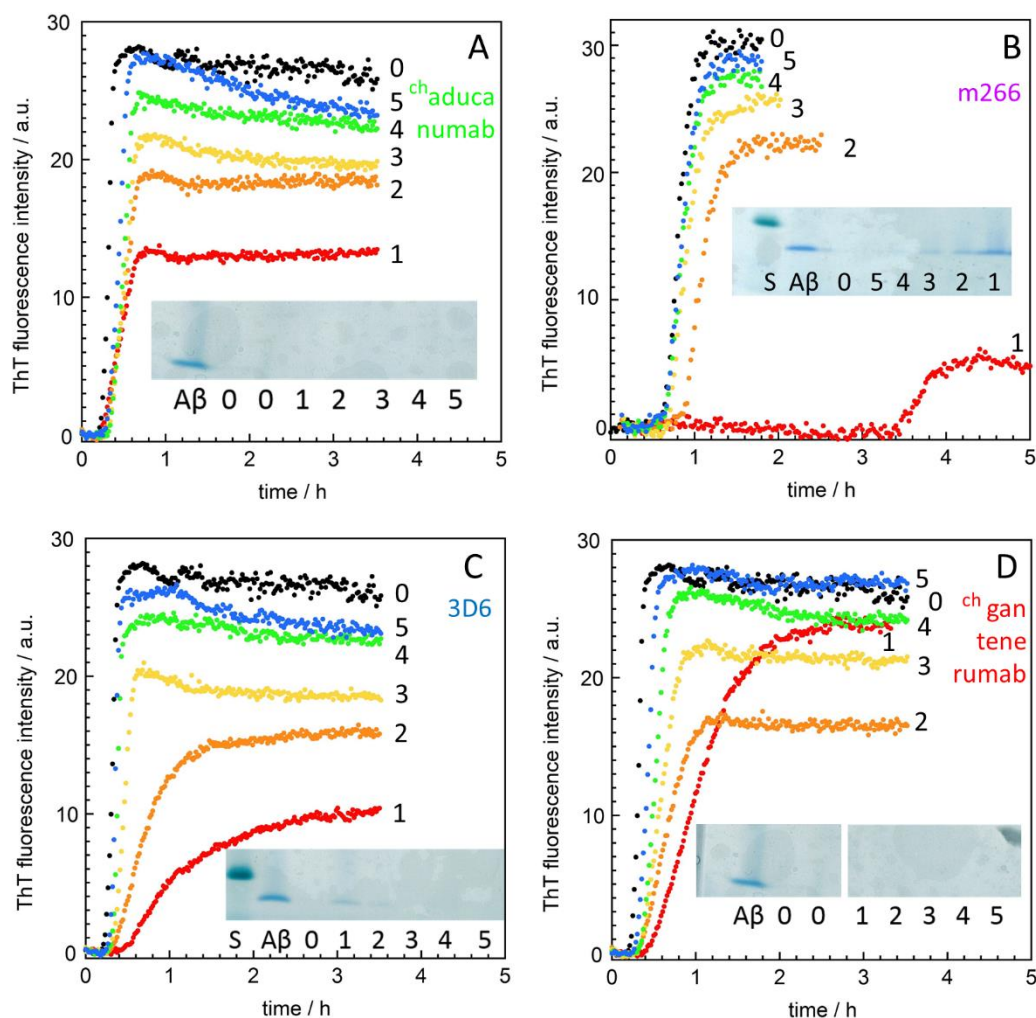
21

Figure S5. Measurements of the amounts of Aβ42 monomers remaining in solution at the end of the aggregation reaction. Here we measured the Aβ1-42 monomers remaining in solution after reaching the ThT plateau in the presence of antibodies that cause a drop in final ThT intensity. Five antibody concentrations were tested (serial dilution 1:1 from 500 or 1000 nM and down). Sample from multiple wells (300-400 μl) were collected after reaching the ThT plateau and fibrils were removed by centrifugation. A small sample (10 μl) from the top of the supernatant was analysed using SDS PAGE (with the standard, S, in panel C and B at 10 kDa). Lane Aβ shows monomers before aggregation, the lane labeled 0 shows the remaining monomer at the plateau for Aβ1-42 alone. Lanes 1-5 correspond to serial dilutions of antibody, with the highest concentration in lane 1 corresponding to 500 nM antibody (chaducanumab, 3D6 and chgantenerumab) or 1 μM antibody (m266). Remaining Aβ1-42 monomers at the plateau are clearly detected with 1 μM, 500 nM and 250 nM m266, and with 500 nM and 250 nM 3D6. Faint Aβ1-42 bands are seen with 125 nM m266 and 125 nM 3D6. Thus, the reduced ThT intensity at the plateau intensity is, at least in part, due to less monomer being consumed in the reaction when high concentration of m266 or 3D6 are present. No Aβ1-42 monomer is detected by this method at the plateau in the presence of chaducanumab or chgantenerumab, indicating that the effect on the ThT plateau intensity is not due to less monomer being consumed in the reaction. Instead, it is likely an effect of these antibodies interfering with the ThT signal. All data were acquired using Aβ1-42 at 37 °C under quiescent conditions in 20 mM Hepes/NaOH, 140 mM NaCl, 1 mM CaCl2, pH 8.0 in PEGylated plates.
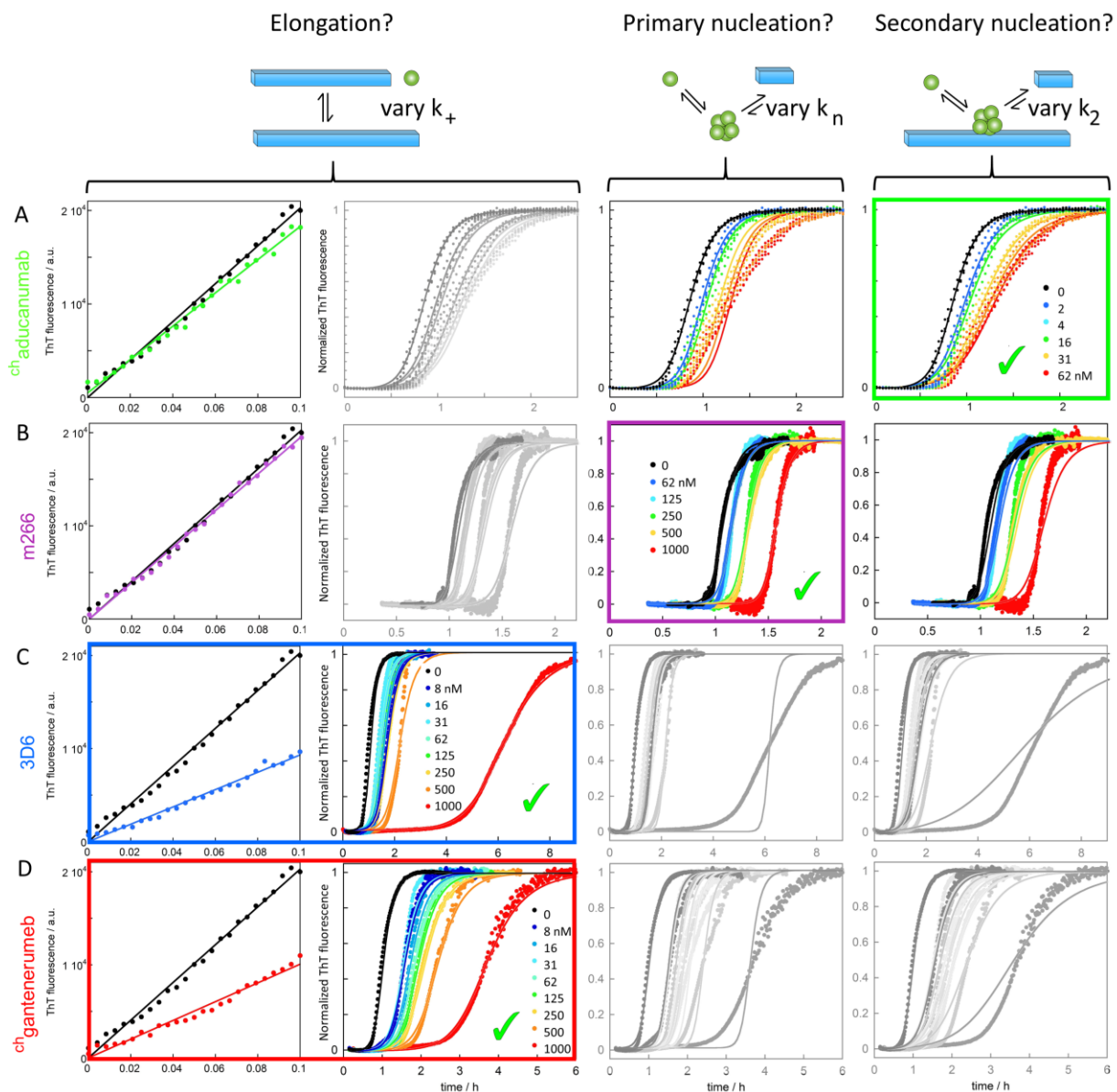
22

Figure S6. Effects of the antibodies on the aggregation kinetics of Aβ1-42 in CSF. ThT fluorescence as a function of time for reactions starting from 6 μM Aβ1-42 in 66% CSF, 20 mM HEPES/NaOH, 140 mM NaCl, 1 mM CaCl$_2$, pH 8.0 in the absence and presence of ^{ch}aducanumab (A), m266 (B), 3D6 (C) or ^{ch}gantenerumab (D). The colour codes for the antibody concentrations are given in nM in each panel. The left column shows data obtained in the presence of 30% preformed seeds, with linear fits, and the following three columns show non-seeded data fitted three times with the selective variation of one rate constant in each column. For ^{ch}aducanumab, the heavy seeded data rule out an effect on k_+, and we can identify a reduction in k_2 as the model which best fits the ^{ch}aducanumab data in CSF; this is verified using light seeding in CSF (Fig. S7). Likewise, for m266 the heavy seeded data rule out an effect on k_+, and we can identify a reduction in k_n as the model which best fits the m266 data in CSF. For 3D6 as well as ^{ch}gantenerumab, the seeded data show an effect on k_+, which indeed explains also the non-seeded data in CSF. Note that the x-axis covers 2.2, 6 or 8 h depending on the magnitude of the effect of each antibody.
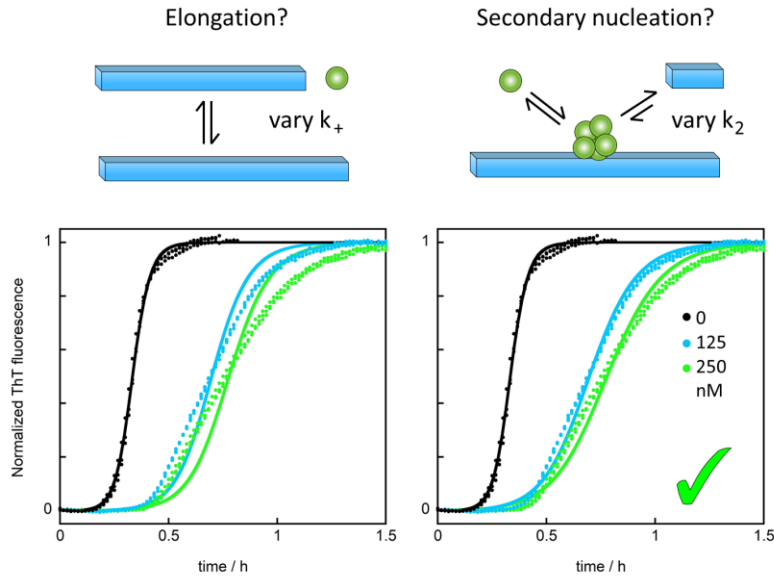
23

Figure S7. Effects of ^{ch}aducanumab on light seeded (2%) aggregation kinetics of Aβ1-42 in CSF. ThT fluorescence as a function of time for reactions starting from 6 µM Aβ1-42 with 120 nM preformed seed fibrils in 66% CSF, 20 mM HEPES/NaOH, 140 mM NaCl, 1 mM CaCl$_2$, pH 8.0 in the absence and presence of ^{ch}aducanumab at 125 and 250 nM. The fits in the left panel assumes a constant value of k_2 and curve-specific values of k_+. The fits in the right panel assumes a constant value of k_+ and curve-specific values of k_2. The inclusion of a low amount of seeds passes primary nucleation and makes the data independent of this step; these data thus validate a reduction of secondary nucleation rate as the primary role of ^{ch}aducanumab in CSF.
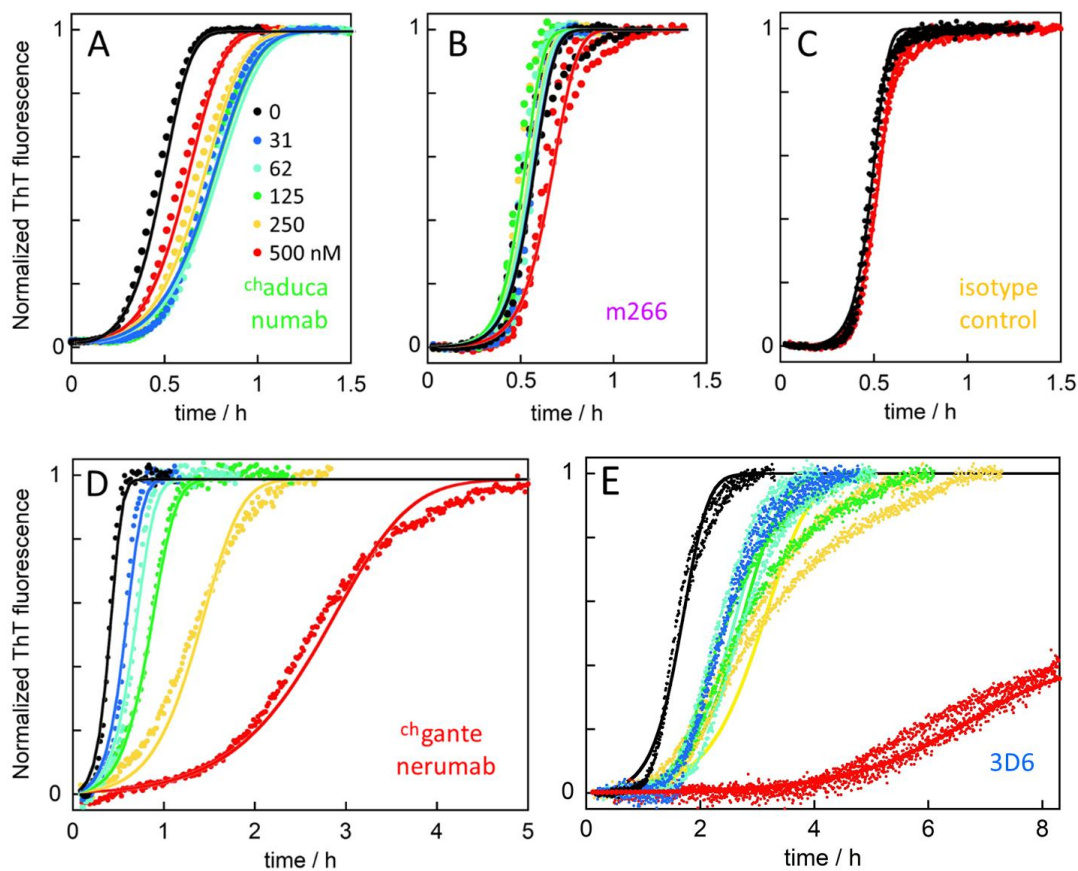
Figure S8. Aggregation kinetics in the presence of preformed seed fibrils at low concentration (2%). Normalized ThT fluorescence as a function of time for reactions starting from 3 to 4 µM Aβ1-42 monomer and 2% (60 to 80 nM) Aβ1-42 fibrils in 20 mM HEPES/NaOH, 140 mM NaCl, 1 mM CaCl$_2$, pH 8.0 in the absence (black) and presence of A) ^{ch}gantenerumab, B) m266, C) isotype control antibody (yellow), D) ^{ch}aducanumab, or E) 3D6 at five concentrations as given by the colour code in panel A. The fitted curves in panels A-C allow only a variation of k$_2$, whereas the fitted curves in panels D,E allow only a variation of k$_+$.
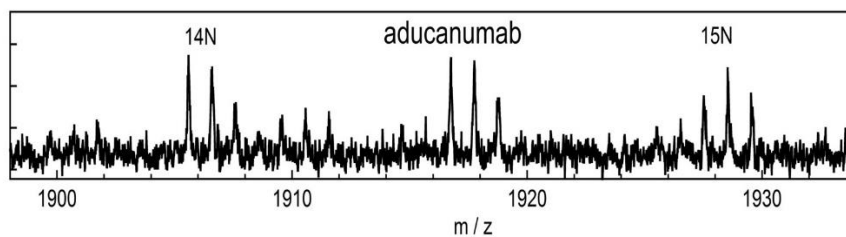
Figure S9. MALDI TOF/TOF analysis of Aβ1-42 in the presence of [ch]aducanumab. Example of a MALDI TOF/TOF spectrum with direct spotting of samples collected at the half-time of aggregation of Aβ1-42 in the presence of [ch]aducanumab.
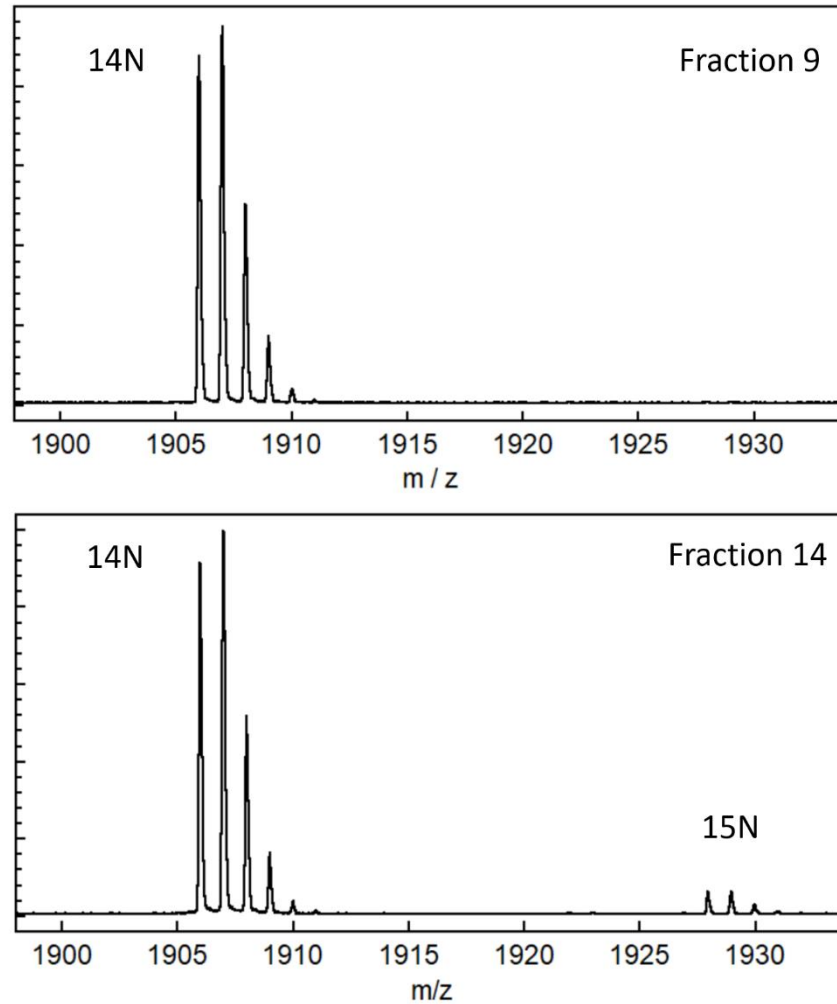
Figure S10. MALDI TOF/TOF analysis of Aβ1-42 in the presence of m266. Example of a MALDI TOF-TOF spectra with HPLC separation before spotting for samples collected at the half-time of aggregation of Aβ1-42 in the presence of m266. In Fraction 9 there is so much 14N peptide that the signal from 15N is suppressed.
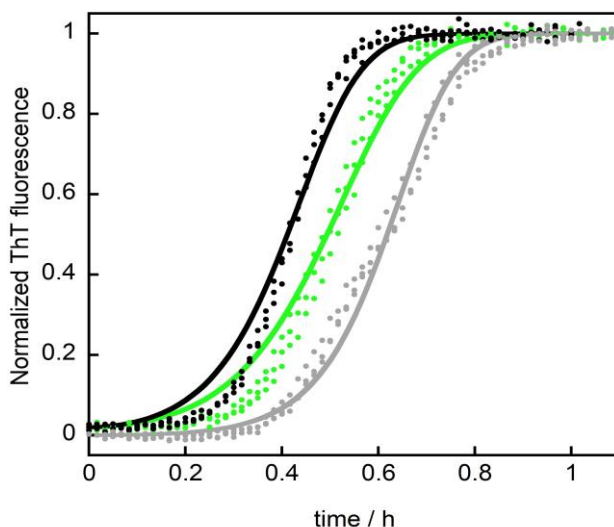
Figure S11. Effects of ^{ch}aducanumab in light seeded (2%) aggregation kinetics of Aβ1-42. ThT fluorescence as a function of time for reactions starting from 3 μM Aβ1-42 in the absence (grey) or presence of 60 nM preformed seed fibrils in 20 mM HEPES/NaOH, 140 mM NaCl, 1 mM $CaCl_2$, pH 8.0. The seeds were made in the absence (black) or presence of chaducanumab (green). The total concentration of ^{ch}aducanumab in the samples for the data shown in green was 6 nM. The fits assume a constant value of k_+ and curve-specific values of k_2. The relative values of k_2 obtained are 1.0 (grey), 1.0 (black) and 0.67 (green). Thus forming the seeds in the presence of ^{ch}aduanumab leads to a 33% reduction in apparent k2, very similar to what we observed with 6 nM ^{ch}aducanumab in the non-seeded data (Fig S4). We conclude that a significant fraction of the inhibitory effect on secondary nucleation originates from interaction of the antibody with fibrillar aggregates.

28
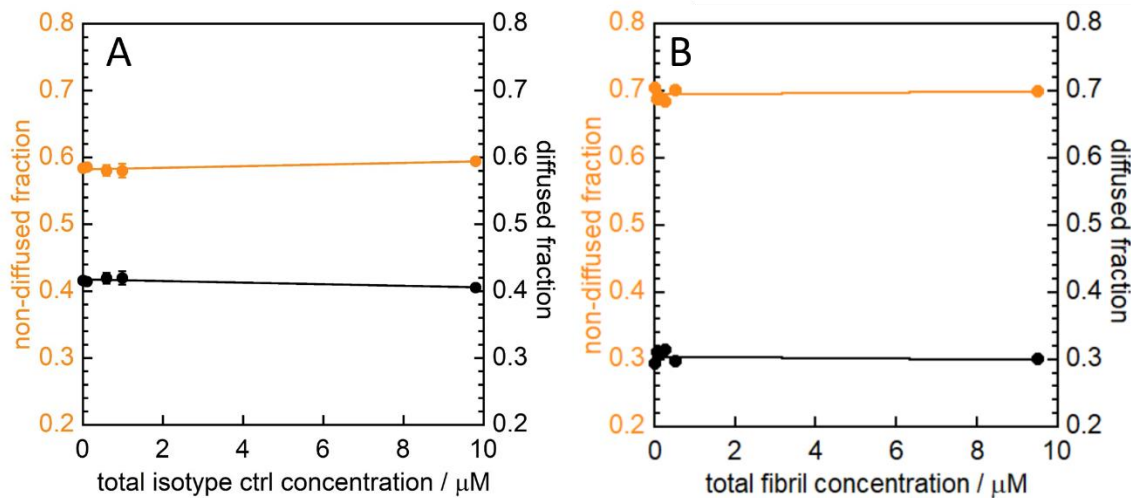
Figure S12. Antibody binding analysis in solution with isotype control antibody.
A) Diffusion of Alexa467-Aβ(MC1-42) in the absence and presence of increasing concentration of isotype control antibody. **B)** Diffusion of Alexa467-labelled isotype control antibody in the absence and presence of increasing concentrations of unlabelled Aβ1-42 fibrils. In both panels are shown the fluorescence intensities in the diffuse and non-diffused half at the channel outlet as a function of total concentration of the non-labelled species. The solid lines are fitted straight lines.

Online Methods

1.1 Chemicals and solutions

All chemicals were of analytical grade. All buffers were filtered (200 nm) and extensively degassed before use. Thioflavin T (ThT) was from CalBiochem and was prepared as a stock solution in water, which was filtered through 200 nm filter and the concentration determined using absorbance. CSF was collected from de-identified healthy donors, pooled and frozen as multiple identical aliquots.

1.2 Expression of Aβ1-42 peptide

Due to the requirement of an ATG start codon yielding an N-terminal Met residue, Aβ1-42 cannot be expressed "as is" and requires a fusion tag. We employed the self-cleavable tag nPro in the form of its EDDIE mutant (31). EDDIE-Aβ1-42 with the amino acid sequence MELNHFELLYKTSKQKPVGVEEPVYDTAGRPLFGNPSEVHPQSTLKLPHDRGEDDIETT LRDLPRKGDCRSGNHLGPVSGIYIKPGPVYYQDYTGPVYHRAPLEFFDETQFEETTKRIG RVTGSDGKLYHIYVEVDGEILLKQAKRGTPRTLKWTRNTTNCPLWVTSC<u>DAEFRHDSG YEVHHQKLVFFAEDVGSNKGAIIGLMVGGVVIA</u>, Aβ1-42 sequence underlined, was expressed from a Pet3a plasmid (purchased from Genscript, Piscataway, New Jersey) in *E. coli* BL21 DE3 PlysS star in overnight express medium (2.5 mM Na$_2$HPO$_4$, 2.5 mM KH$_2$PO$_4$, 12 mM (NH$_4$)$_2$SO$_4$, 1 mM MgSO$_4$, 0.1 g/L glucose, 0.4 g/L lactose, 1 g/L glycerol, 10 g/L NaCl, 10 g/L tryptone, 5 g/L Bacto yeast extract, 50 mg/L ampicillin, 30 mg/L chloramphenicol).

1.3 Purification of Aβ1-42 peptide

Cell pellet from 4 L was sonicated 5 times in 80 mL 10 mM Tris/HCl, 1 mM EDTA, pH 8.5 containing a trace of DNase, with centrifugation at 18,000 xg for 7 min between sonications. The inclusion body pellet (hard and grey, ca. 5-10 mL) after the 5th sonication was dissolved in 150 mL 10 M urea, 10 mM Tris, 1 mM EDTA, 1 mM DTT, pH 8.5 by sonication, grinding, and stirring. The resulting solution (ca. 9.4-9.7 M urea) was diluted with 150 mL 10 mM Tris, 1 mM EDTA, 1 mM DTT pH 8.5 (thus yielding ca. 4.8 M urea) and loaded onto 2 x 20 mL DEAE-sepharose FF columns (GE Healthcare) in tandem. The columns were washed with 100 mL 4 M urea, 10 mM Tris, 1 mM EDTA, 1 mM DTT pH 8.5, and eluted with a 0-0.4 M NaCl gradient in the same buffer. Fractions containing EDDIE-Aβ1-42 were diluted 15 times with 1 M Tris, 1 mM EDTA, 5 mM DTT, pH 7.9 in glass bottles and left at 4°C for 48 h, total volume 1.5 L. During this time EDDIE slowly folds leading to auto-cleavage and release of Aβ1-42. The solution was then dialyzed (in 3.5 kDa MW cutoff dialysis bags that had been boiled 4 times in Millipore water before use) three times against 10 L of 5 mM Tris/HCl, 0.5 mM EDTA, pH 8.5. After this, the solution was poured into a 2 L beaker and supplemented with 50 g Q-sepharose big beads (GE Healthcare, equilibrated in 10 mM Tris/HCl, 1 mM EDTA, pH 8.5) and incubated for 0.5 h in the cold room with stirring using a propeller stirrer. The beads were collected on a Büchner funnel and washed with 200 mL 10 mM Tris/HCl, 1 mM EDTA, pH 8.5, and eluted with 8 x 100 mL 10 mM Tris/HCl, 1 mM EDTA, pH 8.5, 75 mM NaCl. The eluted fractions were examined using SDS PAGE with Coomassie staining. Fractions dominated by Aβ1-42 monomer were lyophilized, dissolved in 10 mL 6 M GuHCl and isolated from residual *E. coli* proteins, aggregates and small molecule contaminants using size exclusion chromatography on a Superdex 75 26/600 column at 4°C. The eluted fractions were examined using UV absorbance, agarose gel electrophoresis and SDS PAGE with Coomassie staining. Fractions corresponding to the center of the Aβ42 monomer peak were

30

pooled, lyophilized, dissolved in 10 mL 6 M GuHCl, 20 mM sodium phosphate, pH 8.5 and subjected to a second round of size exclusion chromatography on a Superdex 75 26/600 column at 4°C. Fractions corresponding to the centre of the Aβ42 monomer peak were pooled, aliquoted and lyophilized.

1.4 Expression and purification of Aβ(M1-42) peptide

Aβ(M1-42) was expressed from a PetSac (derivative of Pet3a) plasmid in *E. coli* BL21 DE3 PlysS star in M9 minimal medium with $^{15}NH_4Cl$ as the only nitrogen source and purified essentially as described (32,12): Cell pellet from 4 L culture was sonicated in 80 mL 10 mM Tris/HCl, 1 mM EDTA, pH 8.5 (buffer A) using a sonicator tip (half horn, 50% duty cycle, maximum output, 30-90 s). This step was performed in a glass beaker surrounded by an ice-water slurry. Inclusion bodies were isolated by centrifugation at 4°C and 18,000 x g for 10 min. Two more rounds of sonication and centrifugation were performed. The inclusion bodies were dissolved in 80 mL buffer A containing 8 M urea and diluted 4-fold in buffer A. 40 mL DEAE cellulose (Whatman DE23, equilibrated in buffer A with 2 M urea) was added, and the slurry was left on ice for 30 min (with periodic stirring using a glass rod). The solution was removed, and the resin washed with buffer A in a Büchner funnel on a vacuum flask, followed by two washes with 100 mL buffer A and elution with 8 x 30 ml buffer A containing 75 mM NaCl. The ion exchange purification was performed in batch mode to avoid concentrating Aβ peptide on the resin. The eluted fractions were examined using SDS PAGE with Coomassie staining. Fractions dominated by Aβ42 monomer were lyophilized, dissolved in 10 mL 6 M GuHCl and isolated from residual *E. coli* proteins, aggregates and small molecule contaminants using size exclusion chromatography on a Superdex 75 26/600 column at 4 °C. The eluted fractions were examined using UV absorbance, agarose gel electrophoresis and SDS PAGE with Coomassie staining. Fractions corresponding to the center of the Aβ(M1-42) monomer peak were pooled lyophilized, dissolved in 10 mL 6 M GuHCl, 20 mM sodium phosphate, pH 8.5 and subjected to a second round of size exclusion chromatography on a Superdex 75 26/600 column at 4°C. Fractions corresponding to the centre of the Aβ42 monomer peak were pooled, aliquoted and lyophilized.

1.5 Generation ad purification of anti-Aβ antibodies

Murine chimeric IgG2a/kappa versions of aducanumab (^{ch}aducanumab), gantenerumab (^{ch}gantenerumab), bapineuzumab (3D6) and solanuzumab (m266) were generated as described (24,33). The variable domain amino acid sequences of bapineuzumab (34) and gantenerumab (4) were selected based on publicly available sequence information, and used to generate murine chimeric analogs. The resultant antibodies contain the variable heavy (V_H) and variable light (V_L) domains of the specific antibody and murine IgG2a/kappa constant heavy and constant light domains. An mIgG2a isotype control antibody P1.17 was generated using DNA cloned from P1.17 hybridoma cell line (ATCC). All antibodies were expressed in CHO cells and purified by protein-A-affinity followed by ion-exchange chromatography. Purified antibodies were frozen as multiple identical aliquots. Prior to setting up the kinetics experiment, these aliquots were further purified using size exclusion chromatography on a 10x300 mm Superdex 200 column eluted in 20 mM HEPES/NaOH, 140 mM NaCl,1 mM CaCl₂, pH 8.0, or in 20 mM sodium phosphate, 0.2 mM EDTA, pH 8.0. Examples of chromatograms are shown in Fig. S2.

1.6 Blinding of antibodies

The experiments were set up blind in the sense that [ch]aducanumab was one of several antibodies that were studied in parallel and their identity was blinded to the person setting up the experiments and analyzing the data. In the experiments with Aβ1-42 at physiological salt buffer and in CSF there were four antibodies (isotype control, [ch]aducanumab, 3D6, [ch]gantenerumab). After un-blinding, the effect of m266 was investigated in physiological salt buffer and CSF.

1.7 Aggregation kinetics experiments. Aliquots of purified lyophilized Aβ1-42 were dissolved in 1 mL 6 M GuHCl, 20 mM sodium phosphate, pH 8.5, and monomer isolated by gel filtration on a Superdex 7510/300 column in 20 mM HEPES/NaOH, 1 mM $CaCl_2$, pH 8.0. The gel filtration step removes traces of pre-existent aggregates and exchanges Aβ peptide into the buffer used in the fibril formation experiments. An example chromatogram is shown in Fig. S2. The peptide concentration was determined from the absorbance of the integrated peak area using $\varepsilon_{280} = 1400$ L $mol^{-1}cm^{-1}$ as calibrated using quantitative amino acid analysis. The monomer generated in this way was diluted with buffer and supplemented with thioflavinT (ThT, Calbiochem) at a final concentration of 10 μM from a 2 mM stock (in water, filtrated through 0.2 μm filter). For experiments with Aβ1-42 at physiological ionic strength, 140 mM NaCl was added after gel filtration from a 4.2 M stock (in 20 mM HEPES/NaOH, 1 mM $CaCl_2$, pH 8.0, filtrated through 0.2 μm filter). For experiments in the presence of CSF, 66% CSF was added from a 100% stock (buffered to pH 8.0 using saturated HEPES solution). The solution with maximum antibody concentration was mixed with $Aβ_{42}$ solution so as to achieve the same $Aβ_{42}$, buffer, salt, $CaCl_2$ or EDTA, ThT and in some cases also CSF concentration as in the antibody-free sample. The antibody-free solution was then mixed in different proportions with the solution with maximum antibody concentration to achieve a dilution series with varying antibody concentration, keeping all other component concentrations constant. All samples were prepared in low-binding tubes (Axygen, California, USA) on ice, using careful pipetting to avoid introduction of air bubbles. Each sample was pipetted into wells of a 96 well half-area plate of PEGylated black polystyrene with a clear bottom (Corning 3881, Massachusetts, USA), 80 μL per well, 3 to 6 replicates of each solution in each plate. The final Aβ42 concentration was between 3 and 4 μM in the kinetic experiments and was constant within each plate. The kinetic assays were initiated by placing the 96-well plate at 37°C under quiescent conditions in a plate reader (Fluostar Omega or Fluostar Optima BMGLabtech, Offenburg, Germany). The ThT fluorescence was measured through the bottom of the plate every 60 s with a 440 nm excitation filter and a 480 nm emission filter. The whole setup with 3-6 replicates per concentration, was repeated at least three times for each combination of antibody, peptide, and buffer or CSF.

1.8 Seeded aggregation kinetics

The seed fibrils were prepared from 5 μM Aβ1-42 monomer solutions (in 20 mM HEPES/NaOH, 1 mM $CaCl_2$, 140 mM NaCl, pH 8.0, 10 μM ThT, as above) by incubation at 37°C under quiescent conditions in a plate reader monitoring ThT fluorescence and collecting the fibrils when the fluorescence reached the post-transition plateau. Fresh Aβ1-42 monomer solutions were prepared as above. The seed fibrils were diluted to two times the final concentration and mixed with equal volume of fresh monomer solution to achieve a final seed concentration of either 30% or 2% of monomer concentration equivalent. Seed-free samples were made for comparison; the monomer solution was mixed with equivalent volume of buffer. Kinetic measurements were made as described above (1.7).

32

1.9 SDS PAGE analysis of monomers

This experiment was aimed at measuring if there is any remaining Aβ1-42 monomer at the ThT plateau in the absence and presence of the antibodies. Samples were collected at the end of the aggregation kinetics, fibrils were removed by centrifugation at 31,500 x g for 2 minutes in a benchtop centrifuge (Hettich Zentrifugen MIKRO 220R) and the supernatant was mixed 1:1 with SDS Loading buffer and analyzed using SDS PAGE on 4-20% polyacrylamide gradient gels (Novex) with a Tris/Bis-Tris Buffer system containing 0.1% SDS. The gels were stained with Coomassie and the intensity of gel bands was compared to that of a monomer standard.

1.10 Kinetic analysis

The aggregation data in the absence and presence of different concentrations of antibodies were normalized and fitted using the Amylofit on-line platform (16) using the following integrated rate law for the normalized aggregate concentration

$$\frac{[M]}{[M]_\infty} = 1 - \left(1 - \frac{[M]_0}{[M]_\infty}\right) e^{-k_\infty t} * \left(\frac{B_- + C_+ e^{\kappa t}}{B_+ + C_+ e^{\kappa t}} * \frac{B_+ + C_+}{B_- + C_+}\right)^{\frac{k_\infty^2}{\bar{k}_\infty \kappa}}$$

[1]

where the parameters are defined as follows

$$\kappa = \sqrt{2[m]_0 k_+ \frac{[m]_0^{n_2} k_2}{1 + [m]_0^{n_2}/K_M}}$$

[2]

$$\lambda = \sqrt{2k_+ k_n [m]_0^{n_c}}$$

[3]

$$C_\pm = \frac{k_+ [P]_0}{\kappa} \pm \frac{k_+ [M]_0}{2[m]_0 k_+} + \frac{\lambda^2}{2\kappa^2}$$

[4]

$$k_\infty = 2k_+ [P]_\infty$$

[5]

$$\bar{k}_\infty = \sqrt{k_\infty^2 - 2C_+ C_- \kappa^2}$$

[6]

$$B_\pm = \frac{k_\infty \pm \bar{k}_\infty}{2\kappa}$$

[7]

In these relations, $[m]_0$ is the initial monomer concentration, $[P]_0$ is aggregate number at the start of the reaction, $[P]_\infty$ is the aggregate number at equilibrium, that is, after reaction completion, $[M]_0$ is the mass concentration of fibrils at the start of the reaction and $[M]_\infty$ is the mass concentration of fibrils at equilibrium. k_n, k_2, k_+ are the rate constants for primary nucleation, secondary nucleation and elongation respectively. K_M is the saturation constant for secondary nucleation and n_c and n_2 are the monomer scalings of primary and secondary nucleation, respectively. The values $n_c = 0.0001$, and $n_2 = 2$ were used for fitting of all aggregation kinetics in 20 mM HEPES/NaOH, 1 mM CaCl$_2$, 140 mM NaCl, pH 8 (18).

Microscopic mechanism of inhibition. The action of an inhibitor can be assessed through the analysis of macroscopic aggregation curves (10,11). Inhibition of primary nucleation (rate constant k_n) causes a lag-phase prolongation with no effect on the transition steepness, thereby delaying the generation of oligomeric species through secondary nucleation (Fig. S1E,H). This type of inhibition requires compounds that bind Aβ monomers, nuclei or other oligomers (11,25-27). By contrast, inhibition of secondary nucleation (with rate constant k_2) causes little lag-phase extension but a reduction of the transition slope (Fig. S1D,G). This route for therapeutic intervention may significantly reduce toxicity (10), and requires inhibitors that block the catalytic surface of fibrils,

33

or bind to on-pathway oligomers to prevent their conversion to fibrils (10-12,25,28,29). Finally, inhibition of elongation (with rate constant k_+) causes both a lag-phase extension and a reduction in transition slope (30), an effect that may increase toxicity over time (10, Fig. S1F,I). When the ends of fibrils are blocked, a larger fraction of the monomers bind to their sides, where secondary nucleation and oligomer generation is catalyzed.

1.11 Oligomer size distribution and concentration

The concentration of oligomers and their size distribution was estimated at $t_{1/2}$, the point in time where half the monomers were converted to fibrils (12,19). Aβ1-42 monomers were isolated by gel filtration in 20 mM HEPES/NaOH, 1 mM CaCl$_2$, pH 8.0, followed by addition of 140 mM NaCl from a concentrated stock. Solutions containing 5 µM monomer and 100 nM antibody (isotype control, [ch]aducanumab, [ch]gantenerumab, m266 or 3D6) were prepared in the same buffer containing 1 µM thioflavin T. The reaction was followed in PEGylated plates (Corning 3881), 100 µl per well, by monitoring ThT fluorescence as described above. The reaction was stopped at $t_{1/2}$, i.e. when the ThT fluorescence reached half-way in between the starting baseline and the final plateau. Solution from 12 wells was combined and centrifuged for 2 minutes at 30,500 x g in a benchtop centrifuge (Hettich Zentrifugen MIKRO 220R). The top 1 mL of the supernatant was injected on a Superdex 75 10/300 column eluted in 20 mM ammonium acetate, pH 8.5, and 1 mL fractions were collected during elution. Each gel filtration fraction was lyophilized, dissolved in 10 µl water, supplemented with 1 pmol ^{15}N-Aβ(M1-42) and subjected to digestion with AspN protease overnight. The sample was concentrated using a C18 zip tip and spotted (0.5 µl) on a steel plate, followed by application of 0.5 µl α-Cyano-4-hydroxycinnamic acid matrix solution and mass spectrometric analysis using an Autoflex Speed Matrix Assisted Laser Desortion Ionization (MALDI) Time-of-Flight (TOF)/TOF system (Bruker Daltonics). In cases of poor signal to noise or antibody fragment overlap, samples were separated by HPLC before spotting on the steel plate before analysis by MALDI-TOF/TOF or were analysed by electrospray ionization (ESI) mass spectrometry using an Orbitrap instrument. The relative intensity of the peaks at 1906 (^{14}N-Aβ7-22, DSGYEVHHQKLVFFAE) and 1928 (^{15}N-Aβ7-22 isotope standard), was used to estimate the oligomer concentration in each fraction.

1.12 Alexa-647 labelling of peptides and antibodies

Aβ(MC1-42), a mutant with an extra Cys residue placed between the starting Met and Asp1 was used for fluorophore labelling (35). An aliquot of purified peptide monomer was dissolved in 6 M GuHCl, 10 mM DTT, pH 8.5, incubated 1 h and the monomer was isolated by gel filtration in 20 mM sodium phosphate buffer, pH 8.0. Two molar equivalents of Alexa-647 C$_2$ maleimide (Thermo Fisher A20347) were added from a concentrated stock in DMSO. The solution was incubated overnight in darkness on ice. Labelled monomer was isolated from free dye by two rounds of gel filtration in 20 mM sodium phosphate buffer, pH 8.0. Antibodies were labelled by mixing with Alexa-647 N-hydroxy succinimidyl ester (Thermo Fisher A20006) after gel filtration of each antibody in PBS. Two molar equivalents of Alexa-647 were added to each antibody, and the solutions were incubated for 2 h at 4°C, followed by gel filtration twice to remove free dye. The absence of free dye was confirmed using microfluidic diffusional sizing with fluorescence detection using a Fluidity One-W instrument (Fluidic Analytics Ltd, Cambridge, UK)

1.13 Binding measurements using microfluidic diffusional sizing (MDS)

Binding interactions in solution were assessed through diffusion measurements under laminar flow in a microfluidic device using a Fluidity One-W instrument (Fluidic Analytics Ltd, Cambridge, UK). The smaller of the two interacting species was used in labelled format. Thus Alexa-467-Aβ_{42} was used to study interactions between peptide monomers and antibodies, and Alexa-467-antibodies were used to study the interaction between antibodies and Aβ1-42 fibrils. Alexa647-Aβ(MC1-42) monomer was isolated by SEC and flash-frozen or kept on ice until use. Unlabelled Aβ1-42 fibrils were formed quiescent at 37 °C in PEGylated plate wells (Corning 3881) from monomer. After formation the fibrils were sonicated (20/20 sec break cycles) for 6 min on ice and shaken for 30 min at 1800 rpm to provide ca. 50 nm diffusible fibrils for the binding experiments. The labelled species was combined with unlabelled binding partner, and incubated for 15 minutes before the diffusion measurements. All binding measurements were performed at 27-28 ˚C in PBS, pH 7.8. The sample was injected in one half of the channel and at the outlet, the fractional fluorescence intensity in the two halves of the channel were analysed separately, F_N representing the non-diffused fluorescent species and F_D the diffused fluorescent species.

Equilibrium binding parameters (affinity and stoichiometry) were obtained by fitting directly to the raw data. Because relatively dilute solutions used, activities were replaced with concentrations and the apparent dissociation constant K_D was estimated by global non-linear regression to the measured quantities, F_D and F_N, using the following equations

$$F_D = F_{D1} + (F_{D2} - F_{D1}) * \frac{0.5(n\,L_{tot} - K_D - C_P) + \sqrt{(0.25(n\,L_{tot} - K_D - C_P)^2 + n\,L_{tot}\,K_D)}}{K_D + 0.5(n\,L_{tot} - K_D - C_P) + \sqrt{(0.25(n\,L_{tot} - K_D - C_P)^2 + n\,L_{tot}\,K_D)}}$$

[8]

$$F_N = F_{N1} + (F_{N2} - F_{N1}) * \frac{0.5(n\,L_{tot} - K_D - C_P) + \sqrt{(0.25(n\,L_{tot} - K_D - C_P)^2 + n\,L_{tot}\,K_D)}}{K_D + 0.5(n\,L_{tot} - K_D - C_P) + \sqrt{(0.25(n\,L_{tot} - K_D - C_P)^2 + n\,L_{tot}\,K_D)}}$$

[9]

where C_P is the total concentration of labelled protein (monomer or antibody), F_{D1} and F_{N1} are the intensities of labelled protein in the respective half of the channel. F_{D2} and F_{N2} is the intensity of labelled protein-ligand complex (monomer-antibody or antibody-fibril) in the respective half of the channel, and n is the stoichiometry of the interaction. For data with Alexa467-labelled Aβ_{42} monomer, n was fixed to 2, while F_{D1}, F_{D2} and K_D were fitted parameters. For data with Alexa467-labelled antibodies, n, F_{N1}, F_{N2} and K_D were fitted parameters.

After fitting, the fractional saturation of the labelled species, Q, was calculated from each data point, F_D or F_N, using the fitted values of F_{D1} and F_{D2}, or F_{N1} and F_{N2} as follows

$$Q = \frac{F_D - F_{D1}}{F_{D2} - F_{D1}}$$

[10]

35

$$Q = \frac{F_N - F_{N1}}{F_{N2} - F_{N1}} \qquad\qquad\qquad\qquad [11]$$

The average of these two values was plotted versus free ligand concentration, which was calculated at each total concentration of added ligand, C_L, as follows

$$[L] = 0.5(n\, L_{tot} - K_D - C_P) + \sqrt{(0.25(n\, L_{tot} - K_D - C_P)^2 + n\, L_{tot}\, K_D)}$$

[12]

using in the case of Alexa647-Aβ_{42} interacting with antibody the fitted value of K_D and the fixed value of n and C_P, and in the case of Alexa647-antibody interaction with fibrils, the fitted values of n and K_D and the fixed value of C_P.

Based on the ratio of F_N and F_D, the instrument reports an apparent hydrodynamic radius of the fluorescently labelled species, the principles of which have been described previously (20,21).

1.14 Comparison with clinical data

Clinical data was collated for each of the antibodies from references (3,5-7). The data related to phase 3 clinical trials for each of the antibodies other than aducanumab. For aducanumab, only the phase 1b clinical data were available. Where results for multiple dose levels were presented, data for the highest dose cohort was used in this analysis.

PET measurements of amyloid clearance: Changes in SUVr PET values were reported relative to the baseline at the start of each trial. The values plotted for clearance correspond to:

Relative reduction in PET SUVr = [(Mean SUVr change for placebo group) - (Mean SUVr change for treated group)]/(Baseline PET SUVr at start of trial)

where the denominator was very similar for the placebo and treated groups within each trial. We note that the observed correlation between clearance and fibril binding is maintained if a cut-off defining amyloid negative scans is included for the PET SUVr values.

Cognitive measurements: Changes in Clinical Dementia Rating–Sum of Boxes (CDR-SB) were reported in the trials for all four antibodies. The values plotted as cognitive improvement correspond to:

Cognitive improvement = (Mean CDR-SB change for placebo group) - (Mean CDR-SB change for treated group)

Fraction antibody bound: We estimated the fraction of Aβ monomers in fibrillar form that are bound at a concentration of 1 nM antibody (24). This measure was calculated as ([A]/n)/([A]+K_D), where [A] = 1 nM, and K_D and the stoichiometry, n, are the measured binding parameters for fibrils from Fig. 3.

36

Relative oligomer flux: We estimated the relative change in the oligomer flux from secondary nucleation for patients treated with each antibody over the course of the published clinical trials, accounting for any changes in the flux in the corresponding placebo groups. The oligomer flux from secondary nucleation depends on the rate constant k_2 for this process, the catalytic fibril surface area which is proportional to the aggregate load, and the free monomer concentration. We assumed that the concentration of monomers does not vary significantly over the course of the clinical trials, such that the relative oligomer flux can be estimated as:

Relative oligomer flux = $(k_2^{Antibody}/k_2^{No\ Antibody})$ ∗ [1 – (Predicted fraction reduction in PET SUVr)]

where $k_2^{No\ Antibody}$ is the value of k_2 in the absence of antibody and $k_2^{Antibody}$ is the value of k_2 in the presence of 1nM antibody (24), calculated from the data in Fig. 1; predicted fraction reduction in PET SUVr is the value for each antibody from the straight line fit in Fig. 4A. We note that the observed correlation between relative oligomer flux and cognitive improvement is maintained if a cut-off defining amyloid negative scans is included for the PET SUVr values.

Additional References

25. Aprile, F.A. *et al*. Selective targeting of primary and secondary nucleation pathways in Aβ42 aggregation using a rational antibody scanning method. *Sci. Adv.* **3**, e1700488 (2017).

26. Habchi, J. *et al*. An anticancer drug suppresses the primary nucleation reaction that initiates the production of the toxic Aβ42 aggregates linked with Alzheimer's disease. *Sci. Adv*. **2**, e1501244 (2016).

27. Månsson, C. *et al*. Interaction of the molecular chaperone DNAJB6 with growing amyloid-beta 42 (Aβ42) aggregates leads to sub-stoichiometric inhibition of amyloid formation. *J. Biol. Chem*. **289**, 31066-31076 (2014).

28. Munke, A. *et al*. Phage display and kinetic selection of antibodies that specifically inhibit amyloid self-replication. *Proc. Natl. Acad. Sci. U. S. A*. **114**, 6444-6449 (2017).

29. Habchi, J. *et al*. Systematic development of small molecules to inhibit specific microscopic steps of Aβ42 aggregation in Alzheimer's disease. *Proc. Natl. Acad. Sci. U. S. A*. **114**, E200-E208. (2017).

30. Bove-Fenderson,E., Urano, R., Straub, J.E. & Harris D.A. Cellular prion protein targets amyloid-β fibril ends via its C-terminal domain to prevent elongation. *J. Biol. Chem*. **292**, 16858-16871 (2017).

31. Kaar, W. *et al*. Refolding of Npro fusion proteins. *Biotechnol Bioeng*. **104**, 774-784 (2009).

32. Walsh, D.M. *et al*. A facile method for expression and purification of the Alzheimer's disease-associated amyloid beta-peptide. *FEBS J*. **276**, 1266-1281 (2009).

33. Bard, F. *et al*. Peripherally administered antibodies against amyloid β peptide enter the central nervous system and reduce pathology in a mouse model of Alzheimer disease. *Nat. Med.* **6**, 916–919 (2000).

34. Panza, F. *et al*. Bapineuzumab: anti-β-amyloid monoclonal antibodies for the treatment of Alzheimer's disease. *Immunotherapy* **2**, 767-782 (2010).

35. Nasir, I., Linse, S. & Cabaleiro-Lago, C. Fluorescent filter-trap assay for amyloid fibril formation kinetics in complex solutions. *ACS Chem Neurosci.* **6**, 1436-1444 (2015).